Coherent Control of Two-level Systems with Periodic N-Steps Driving Fields

Zhi-Cheng Shi,[1,2] Ye-Hong Chen,[3] Wei Qin,[3] Yan Xia,[1,2,*] X. X. Yi,[4,†] Shi-Biao Zheng,[1,2] and Franco Nori[3,5]

[1]*Department of Physics, Fuzhou University, Fuzhou 350002, China*
[2]*Fujian Key Laboratory of Quantum Information and Quantum Optics, Fuzhou University, Fuzhou 350116, China*
[3]*Theoretical Quantum Physics Laboratory, RIKEN Cluster for Pioneering Research, Wako-shi, Saitama 351-0198, Japan*
[4]*Center for Quantum Sciences and School of Physics,*
Northeast Normal University, Changchun 130024, China
[5]*Department of Physics, University of Michigan, Ann Arbor, Michigan 48109-1040, USA*

In this work, we derive the exact solutions of the dynamical equation, which can describe all two-level Hermitian systems driven by periodic N-steps driving fields. The solutions are a set of quasi-periodic functions, and the expressions of the amplitudes and phases are obtained in the frequency-domain. Particularly, we develop a general formalism for the effective Hamiltonian without any approximations, and give the validity range according to the transition probability of the micromotion operator. With the guidance of the exact solutions and the effective Hamiltonian, we find that the coherent destruction of tunneling phenomenon, the resonance phenomenon, and the beat-frequency phenomenon can emerge in this system. Finally, some applications are demonstrated in quantum information processing by periodic N-steps driving fields.

Introduction.—Over the past decade, periodically driven systems have become the focus of intensive research, owing to the appearance of several interesting phenomena, including coherent destruction of tunneling [1, 2], dynamical freezing and localization [3–13], etc. Those phenomena are usually inaccessible for undriven systems. More importantly, periodic driving fields can be exploited to control quantum dynamics, and then perform quantum information processing. For instance, multiphoton resonances can be effectively suppressed by periodic driving fields associated with pulse-shaping techniques [14], and sinusoidal driving fields have been used to prepare entangled states and implement quantum gates [15–20]. In many-body systems, periodic driving fields also provide a new method for coherent quantum manipulations [21–23].

As is well known, it is hard to obtain the exact dynamics of general time-dependent driven systems, even in the simplest two-level system (TLS) [24–29]. Until now, the exact solution is only acquired in a handful of special cases, such as the well-known Landau-Zener model [30, 31]. Thus, the universal treatment of periodically driven systems to derive a time-independent effective (Floquet) Hamiltonian, so that one can discover some nontrivial physical properties (e.g., dynamical localization [11–13]). This also brings about a drawback that researchers always ignore or hardly understand some other intriguing phenomena (e.g., the beat phenomena in this Letter). The reason is that the effective Hamiltonian cannot fully describe the actual dynamics of systems.

Recently, a general formalism [32], which extends the method introduced in Ref. [33], has been proposed to describe periodic-square-wave driven systems [34–38]. More specifically, the dynamics of periodic-square-wave driven systems can be divided into two parts: (*i*) the long time-scale dynamics governed by an effective Hamiltonian and (*ii*) the short time-scale dynamics

governed by a micromotion operator. Nevertheless, this formalism is only suitable for the off-resonance regime and applicable to a specific square-wave that possesses the same time intervals. Afterwards, this method is generalized to the resonant regime by performing a time-dependent unitary transformation [39]. Note that it might be invalid as well when the frequency of driving fields is arbitrary. Therefore, the main motivation of this work is to give the accurate effective Hamiltonian and the micromotion operator for an arbitrary parameter range [including the strongly (weakly) coupled systems and the arbitrary frequency of driving fields], discover the beat phenomena, and then seek the possibility of controlling quantum dynamics via square-wave driving fields.

In this work, by giving the exact expression of the evolution operator, we systematically solve a class of dynamical equations, which can describe all TLSs driven by periodic N-steps driving fields. Note that the exact solution is valid for full parameter range since we do not make any approximations for the TLS and the driving fields. Moreover, we derive the general expressions of the amplitudes and phases in the frequency-domain. It is interesting to find that there always exists the beat-frequency-like phenomena (hereafter we call it "beat phenomena") in the time-dependent transition probability, when choosing specific parameters. Besides, we do not require an extra operator (cf. Refs. [32, 33]) to describe the long time-scale dynamics with different starting time of the driving fields, since our effective Hamiltonian contains relevant information.

Physical model.—We consider a TLS interacting with a driving field. The dynamics is governed by the following Hamiltonian ($\hbar = 1$)

$$
\begin{aligned}
H(t) &= \mathcal{E}(t) \cdot \boldsymbol{\sigma} + \frac{\Delta(t)}{2}\boldsymbol{I} \\
&= \Delta(t)|2\rangle\langle 2| + \left[\epsilon(t)e^{i\theta(t)}|1\rangle\langle 2| + \text{H.c.}\right],
\end{aligned} \quad (1)
$$

where $\mathcal{E}(t) = (\epsilon(t)\cos\theta(t), \epsilon(t)\sin\theta(t), -\Delta(t)/2)$, $\boldsymbol{\sigma} = (\sigma_x, \sigma_y, \sigma_z)$ represents the Pauli matrices, and $\boldsymbol{I}$ is the identity matrix. The first and second terms of the second line can be regarded as the time-dependent energy bias and tunneling amplitude of the TLS, respectively [2, 24, 25, 40]. Actually, this Hamiltonian can describe most quantum systems with a two-level structure, and the coefficients $\Delta(t)$, $\epsilon(t)$, and $\theta(t)$ represent different physical quantities in different systems. For example, $\Delta(t)$ and $\epsilon(t)$ represent the quasiparticle momenta in condensed-matter systems [14, 41, 42], the detuning and the Rabi frequency in an atomic system interacting with a laser field [43], or the dc and ac flux biases in superconductor qubits [44, 45], etc. We assume that all the coefficients are adjustable.

Assume that the periodic driving field has the form of repeated N-steps sequence $S_N : \{H_1, H_2, ..., H_N\}$. For the nth step, the interaction time between the TLS and the driving field is τ_n, and the Hamiltonian H_n becomes $(n = 1, ..., N)$

$$H_n = \Delta_n |2\rangle\langle 2| + \left(\epsilon_n e^{i\theta_n}|1\rangle\langle 2| + \text{H.c.}\right). \quad (2)$$

As a result, the period of N-steps sequence is $T = \sum_{n=1}^{N} \tau_n$. Note that the parentheses are omitted hereafter for the sake of clarity if the parameters are time-independent. In this work, we do not restrict the values of each duration τ_n as well as $\Delta(t)$ and $\epsilon(t)$. Therefore, the period T and other parameters can be arbitrary. As a result, because no quantities in $H(t)$ can be treated as perturbations, both the Floquet theory [2, 46, 47] and the rotating-wave approximation [48–52] are invalid to calculate the effective Hamiltonian for this system.

Expressions for the micromotion operator and effective Hamiltonian.—Different from the partitioning introduced in Refs. [32, 33], we directly divide the evolution operator at arbitrary final time $t_f = t + \mathcal{N}T$ ($t < T$, $\mathcal{N} = 0, 1, 2, ...$) into two factors: $\mathbb{U}(t_f) = \mathbb{U}(t)\mathbb{U}(\mathcal{N}T) \equiv \exp[-i\mathcal{M}(t)]\exp(-iH_{\text{eff}}\mathcal{N}T)$. Here, the time-dependent micromotion operator $\mathcal{M}(t)$ and the time-independent effective Hamiltonian H_{eff} describe the short time-scale ("fast" part) dynamics and the long time-scale ("slow" part) dynamics of the periodic N-steps driven system, respectively. The eigenvalues of H_{eff} are referred to as the quasienergies of the system. To obtain the solutions of $\mathcal{M}(t)$, first of all, we need to calculate the concrete form of the evolution operator $\mathbb{U}(t)$. Then, by reversely solving the equation $\exp[-i\mathcal{M}(t)] = \mathbb{U}(t)$, we can obtain the expression for $\mathcal{M}(t)$, which reads,

$$\mathcal{M}(t) = \Delta_{\mathcal{M}}(t)|2\rangle\langle 2| + \left[\epsilon_{\mathcal{M}}(t)e^{i\theta_{\mathcal{M}}(t)}|1\rangle\langle 2| + \text{H.c.}\right], \quad (3)$$

where $\Delta_{\mathcal{M}}(t) = 2B_n(t)\arccos A_n(t)/\sqrt{1 - A_n(t)^2}$, $\epsilon_{\mathcal{M}}(t) = \sqrt{C_n(t)^2 + D_n(t)^2}\arccos A_n(t)/\sqrt{1 - A_n(t)^2}$, $\theta_{\mathcal{M}}(t) = \arctan[C_n(t)/D_n(t)]$. Due to the tedious expressions of the coefficients $A_n(t)$, $B_n(t)$, $C_n(t)$, and $D_n(t)$, we present them in Supplemental Material [53].

To derive the effective Hamiltonian H_{eff}, we need to exploit the primitive definition $\mathbb{U}(T) \equiv \exp(-iH_{\text{eff}}T)$, where $\mathbb{U}(T)$ is the evolution operator within one period. One can find that H_{eff} is a special case of the micromotion operator $\mathcal{M}(t)$, which satisfy $H_{\text{eff}} = \mathcal{M}(T)/T$. Thus, the form of H_{eff} is

$$H_{\text{eff}} = \Delta_{\text{eff}}|2\rangle\langle 2| + \left(\epsilon_{\text{eff}}e^{i\theta_{\text{eff}}}|1\rangle\langle 2| + \text{H.c.}\right), \quad (4)$$

where $\{\Delta_{\text{eff}}, \epsilon_{\text{eff}}, \theta_{\text{eff}}\} = \{\Delta_{\mathcal{M}}(T), \epsilon_{\mathcal{M}}(T), \theta_{\mathcal{M}}(T)\}/T$. With the evolution operators $\mathbb{U}(t)$ and $\mathbb{U}(T)$, we naturally obtain the exact expression of the evolution operator $\mathbb{U}(t_f)$ for this system [53].

For the general situation, the first period of the pulse sequence may have a jump, e.g., the sequence from t_0 to t_1 in Fig. 1(a). When this jump is considered, an additional initial kick is required to describe the dynamics as discussed in Refs. [32, 33], since this jump might affect the long time-scale dynamics [see the solid-curve in Fig. 1(b)]. In contrast, we can integrate
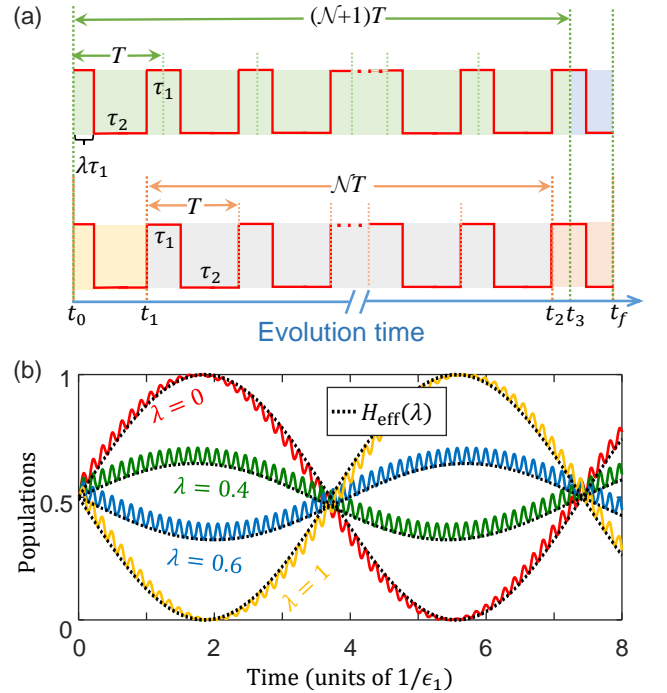

FIG. 1. (a) Schematic diagram of distinct partitions of the same two-steps sequence with period T. The occurrence of the first jump is quantified by λ. In the top panel, the evolution operator is divided into two factors (shaded with different colors): $\mathbb{U}(t_f, t_3)\mathbb{U}(t_3, t_0)$, while it is divided into three factors: $\mathbb{U}(t_f, t_2)\mathbb{U}(t_2, t_1)\mathbb{U}(t_1, t_0)$ in the bottom panel. (b) Population evolution of level $|2\rangle$ for different λ, where the initial state is $(|1\rangle + |2\rangle)/\sqrt{2}$. The black-dotted curves represent the predictions given by the effective Hamiltonian $H_{\text{eff}}(\lambda)$. Each dotted curve almost coincides with the envelope of its solid counterpart, indicating that $H_{\text{eff}}(\lambda)$ contains relevant information caused by different starting time of the driving fields. The parameters chosen here are $\{\epsilon_n/\epsilon_1\} = \{1, 2\}$, $\{\Delta_n/\epsilon_1\} = \{50, 40\}$, and $E_1\tau_1 = E_2\tau_2 = \pi/2$.

this jump into the effective Hamiltonian here, and do not require an additional kick. The result is that different starting time (phases) of the driving fields would lead to different effective Hamiltonians. To address this issue more clearly, we employ a quantity λ to describe this jump [see Fig. 1(a)]. By using another partition of the sequence, we can regard the jump sequence as a complete $(N + 1)$-steps sequence S_{N+1}: $\{H_m, H_{m+1}, ..., H_N, H_1, ...H_m\}$. Here, the final step Hamiltonian is the same to the mth step Hamiltonian with the interaction time $(1 - \lambda)\tau_1$. Then, we readily obtain the effective Hamiltonian $H_{\text{eff}}(\lambda)$ for the jump sequences. It is shown in Fig. 1(b) that the long time-scale dynamics (i.e., the envelope of the solid-curve) caused by different starting time of driving fields are well described by the effective Hamiltonian $H_{\text{eff}}(\lambda)$.

Expressions for the transition probability.—Note that there are two fundamental frequencies in this system: the frequency of the N-steps driving field $\omega_T = 2\pi/T$ and the Rabi frequency of the effective Hamiltonian $\omega_{\text{eff}} = \sqrt{\epsilon_{\text{eff}}^2 + \Delta_{\text{eff}}^2/4}$. We can expand the time-dependent transition probability $P_{1\to2}(t)$ from $|1\rangle$ to $|2\rangle$ using cosine functions with discrete frequencies,

$$P_{1\to2}(t) = \bar{b} + \sum_{l=-\infty}^{\infty} \Big\{ b_l \cos\big[(2\omega_{\text{eff}} + l\omega_T)t - \varphi_l\big]$$
$$+ b_l' \cos\big(l\omega_T t - \varphi_l'\big) \Big\}, \tag{5}$$

where the amplitudes $\{\bar{b}, b_l, b_l'\}$ and the phases $\{\varphi_l, \varphi_l'\}$ are achieved by Fourier transform [53]. We stress that we make no approximations in obtaining the micromotion operator and the effective Hamiltonian given by Eqs. (3)-(4). Hence, Eq. (5) is exact and valid for all parameter ranges, including the (near-) resonance and the large-detuned regimes, as well as for arbitrary values of the period T. Until now, we have given the exact solution of the dynamics of a TLS driven by a periodic N-steps sequence in an arbitrary parameter range. In the following, according to the maximum transition probability $\mathcal{P}_s^{\text{max}}$ ($\mathcal{P}_l^{\text{max}}$) of short (long) time-scale dynamics, we divide the parameter range into two situations and illustrate the dynamical evolution by a two-step sequence, while similar results can be easily obtained for $N > 2$.

(i) $\mathcal{P}_s^{\text{max}} \ll \mathcal{P}_l^{\text{max}}$. In this situation, the micromotion operator $\mathcal{M}(t)$ makes few contributions to the transition process, and the effective Hamiltonian plays a dominant role in the transition process. As a result, the actual dynamics can be well described by the effective Hamiltonian (4) and appear Rabi-like oscillations with the frequency ω_{eff}. The transition formula is truncated by two terms in Eq. (5): the dc term $\bar{b}$ and the term $l = 0$,

$$P_{1\to2}^{\text{eff}}(t) = \frac{\epsilon_{\text{eff}}^2}{2\omega_{\text{eff}}^2} \left(1 - \cos 2\omega_{\text{eff}}t\right). \tag{6}$$

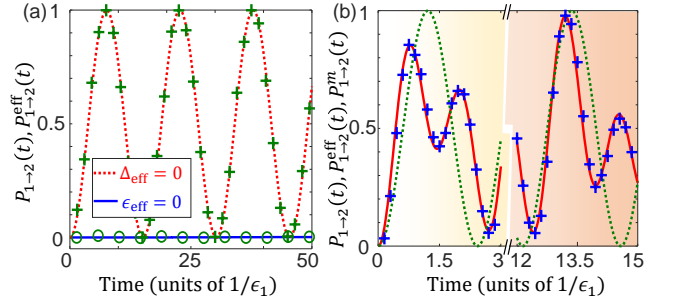

FIG. 2. Time evolution of the transition probability. (a) The green crosses and circles represent the predictions given by $P_{1\to2}^{\text{eff}}(t)$ in Eq. (6). The high-degree overlap between curves and markers demonstrates that the actual dynamics is well described by the effective Hamiltonian (4). In the left panel, we properly choose $\{\epsilon_n/\epsilon_1\} = \{1, 1.8, 1.5, 1.1\}$, $\{\Delta_n/\epsilon_1\} = \{30, 45, 55, 60\}$, $\{\tau_n/10\epsilon_1\} = \{2.09, 1.39, 1.14, 1.045\}$ for the blue-solid curve, and $\{\tau_n/100\epsilon_1\} = \{2, 1, 2, 5.96\}$ for the red-dotted curve. (b) The red-solid-curve represents the actual dynamics of the system and the green-dotted curve (blue crosses) corresponds to the predictions given by Eq. (6) [Eq. (7)]. These results show that the effective Hamiltonian is invalid in this case, while the actual dynamics can be well described by Eq. (7). Here, we properly choose $\{\epsilon_n/\epsilon_1\} = \{1, 2\}$ and $\{\Delta_n/\epsilon_1\} = \{22, 1.6\}$, which satisfy $\Delta_{\text{eff}} = 0$ and H_1 (H_2) is in the large-detuned (near-resonance) regime.

Actually, this situation is the validity scope of the effective Hamiltonian, and the parameter range involves two parts. First, all the Hamiltonians H_n are in the large-detuned regime. Note that most current periodically driven systems [17–20, 54–56] are in this regime. But, in contrast to those systems, the validity of H_{eff} does not depend on the frequency of driving field in the present model. Second, some Hamiltonians H_m are in the (near-) resonance regime, where the interaction time τ_m is short enough (i.e., $E_m\tau_m \ll 1$, $m \subseteq \{1, ..., N\}$). We stress that this regime has been never pointed out before.

According to Eq. (6), we find two phenomena in this system. First, the phenomenon of coherent destruction of tunneling could appear when satisfying the condition $\epsilon_{\text{eff}} = 0$, leading to the forbidden transition between levels [see the blue-solid-curve in Fig. 2(a)]. Second, the resonance (complete) transition between levels could occur when satisfying the resonance condition $\Delta_{\text{eff}} = 0$, as plotted by the red-dotted-curve in Fig. 2(a). Physically, the two phenomena result from the destructive and constructive interference of distinct evolutionary paths [40].

Let us go back to the Landau-Zener model [30, 31, 40]. When a TLS is periodically driven through the energy avoided level crossing (i.e., requiring $\Delta_1\Delta_2 < 0$ in the two-steps sequence), the resonance condition is reduced to $E_1\tau_1 - E_2\tau_2 \simeq k\pi$ (k is an integer), which returns to the results obtained in Ref. [57, 58]. In fact, one can achieve this resonance condition via the frequency-matching from

a physical point of view. First of all, the average energy-level detuning of the TLS is $\bar{E}_T = 2(E_1\tau_1 - E_2\tau_2)/T$, within one period. In order to implement the resonance transition, the frequency ω_T of the driving fields should match this detuning. As a result, it requires $k\omega_T = \bar{E}_T$, which is exactly the resonance condition. Thus one can describe this resonance condition as a $|k|$-photon process.

(ii) $\mathcal{P}_s^{\max} \lesssim \mathcal{P}_l^{\max}$. In this situation, the micromotion operator $\mathcal{M}(t)$ plays an important role in the transition process, leading to the invalidity of the effective Hamiltonian to describe the actual dynamics [as shown by the green-doted curve in Fig. 2(b)]. The parameter range contains some Hamiltonians H_m are in the (near-) resonance regime where the interaction time τ_m is long enough.

Generally speaking, to describe the actual dynamics more accurately, we require to keep more terms in Eq. (5). Without loss of generality, we consider that the Hamiltonian H_1 is in the large-detuned regime ($|\Delta_1| \gg |\epsilon_1|$) and the Hamiltonian H_2 is in the near-resonance regime ($|\Delta_2|/|\epsilon_2| \simeq 0$). Here, we intend to give the empirical expressions for b_{-1} and φ_{-1} [i.e., introducing the extra term $l = -1$ in Eq. (5)], because the exact expression is involved [53]. The modified transition probability can be written as

$$P_{1\to2}^m(t) = \frac{\epsilon_{\mathrm{eff}}^2}{2\omega_{\mathrm{eff}}^2}\Big[1-(1-\lambda)\cos 2\omega_{\mathrm{eff}}t - \lambda\cos 2\omega_{\mathrm{eff}}^- t\Big], \quad (7)$$

where $\lambda = [1 - \mathrm{mod}(E_1\tau_1, \pi)/\pi]\mathcal{P}_s^{\max}$, and $\omega_{\mathrm{eff}}^- = \omega_T/2 - \omega_{\mathrm{eff}}$. The relevant result is shown by the blue crosses in Fig. 2(b), which nearly coincides with the actual dynamics. When both Hamiltonians H_1 and H_2 are in the large-detuned regime, we readily find that $\lambda \simeq 0$, thus reverting back to the dynamics governed by Eq. (6). Therefore, this modified formalism almost fits the full parameter range [53].

Beat phenomena.—In classical mechanics, the beating occurs with two harmonics when the sum of their frequencies is much greater than the difference of their frequencies. To our knowledge, it is hard to observe the beat phenomena in the TLS, since the waveforms of the physical parameters are intricate and singular [53].

According to Eq. (7), if $\lambda = 1/2$, the transition probability would appear beat phenomena. In fact, this is the case that the beating always exists in the N-steps driven system, when at least one Hamiltonian is in the large-detuned (resonance) regime [53]. Then, by modulating the dynamical phases, the transition probability can be approximately described by

$$P_{1\to2}^b(t) = \frac{1}{2}\Big[\sin^2 \varpi_1(t - t_p) + \sin^2 \varpi_1^-(t - t_p)\Big], \quad (8)$$

where the similar frequencies ϖ_1 and ϖ_1^- are closely related to the effective quantity ϵ_{eff}, and t_p is the time-shifting factor. Remarkably, the beat phenomena cannot

be explained by only using the effective Hamiltonian, and this is the reason why scarcely any researches focus on these phenomena in periodically driven systems. Physically, the beating results from the interference effect of the dynamical phases of different Hamiltonians. Moreover, the parity number of N determines the values of the frequencies ϖ_1 and ϖ_1^-. For example, when N is even and n_1 Hamiltonians are in the resonance regime, we have

$$\varpi_1 = \frac{1}{2}\begin{cases} (n_1 - 1)\epsilon_{\mathrm{eff}}^- + (n_1 + 1)\epsilon_{\mathrm{eff}}, & n_1 \text{ is odd}, \\ n_1\epsilon_{\mathrm{eff}}^- + (n_1 - 2)\epsilon_{\mathrm{eff}}, & n_1 \text{ is even}, \end{cases}$$

and

$$\varpi_1^- = \frac{1}{2}\begin{cases} (n_1 + 1)\epsilon_{\mathrm{eff}}^- + (n_1 - 1)\epsilon_{\mathrm{eff}}, & n_1 \text{ is odd}, \\ n_1\epsilon_{\mathrm{eff}}^- + (n_1 + 2)\epsilon_{\mathrm{eff}}, & n_1 \text{ is even}, \end{cases}$$

where $\epsilon_{\mathrm{eff}}^- = \omega_T/2 - \epsilon_{\mathrm{eff}}$. Figure 3 demonstrates one example to observe the beat phenomenon in the periodic two-steps driven system, indicating that the actual dynamics can be well described by Eq. (8).
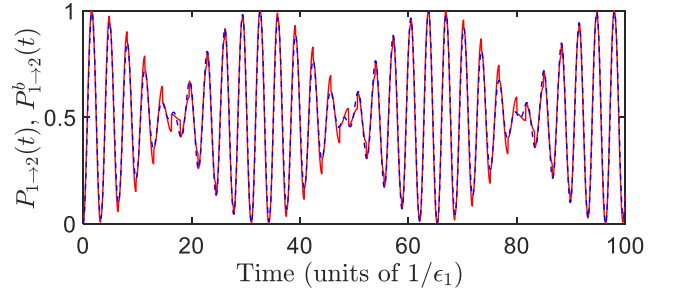

FIG. 3. Beat phenomena in the periodic two-steps driven system. The red-solid curve denotes the actual dynamics and the blue-dashed curve corresponds to the prediction given by Eq. (8). The high-degree overlap between two curves verifies the validity of Eq. (8). We properly choose parameters $\{\epsilon_n/\epsilon_1\} = \{1,2\}$, $\{\Delta_n/\epsilon_1\} = \{0,50\}$, and $E_1\tau_1 = E_2\tau_2 = \pi/2$.

Applications.—The periodic N-steps driving field can be widely used in quantum coherent control, since all kinds of physical quantities can be exploited to manipulate quantum states. For example, to implement the complete transition from $|1\rangle$ to $|2\rangle$, we can only control the coupling strength $\epsilon(t)$ in the resonance pulses. However, when employing the periodic N-steps driving field, we can adopt multiple choices to design the physical parameters, such as the detuning $\Delta(t)$, the coupling strength $\epsilon(t)$, and the phase $\theta(t)$. By modulating the values of $\{\Delta(t), \epsilon(t), \theta(t)\}$, one can accurately control the transition time between the levels. Moreover, one can also implement the forbidden transition between levels by two resonance pulses, and the parameters should satisfy $\theta_2 = \theta_1 + \pi$ and $\Omega_2\tau_2 = \Omega_1\tau_1 \ll \pi/2$.

The beat phenomena observed in the periodic N-steps system could find potential applications in homodyne

detection. Physically, some quantities, such as phase, are hard to directly measure. Besides, in strong-coupling TLSs, the Rabi oscillation is too fast to measure the coupling strength by population evolution. According to Eq. (8), different physical quantities are closely interconnected, and there are two different frequencies: the high-frequency component $(\varpi_1 + \varpi_1^-)$ and the beat frequency $(\varpi_1 - \varpi_1^-)$. Thus, it is convenient to transform the unaccessible direct-measurement physical quantity (e.g., the phase) into the beat signal, enabling it to be easily measured by detecting the envelope waveform of the beat signal. Furthermore, the envelope changes slowly so that we can directly measure the coupling strength by Eq. (8) in strong-coupling TLSs. At the same time, the measurement precision is correspondingly improved due to the beat signal. Another application is that one is available to design the feedback system to keep the stability of physical quantities by detecting the variation of the beat signal in quantum systems.

Summary.—We have presented the solution of the evolution operator for a full parameter range in the periodic N-steps driven TLS. The actual dynamics of the TLS can be expanded by the superposition of cosine functions with discrete frequencies, while the predicted dynamics governed by the effective Hamiltonian only contains one fundamental frequency. We also derive the form of effective Hamiltonian for different starting time of driving fields. Particularly, we give the validity scope of the effective Hamiltonian, i.e., either all Hamiltonians in the large-detuned regime or some Hamiltonians in the (near-) resonance regime where the interaction time is short enough. When the micromotion operator contributes to the evolution, we can introduce a modified transition probability to describe the actual dynamics. Moreover, we have demonstrated that the beat phenomenon always exists in the N-steps driven TLS, which is hardly found by the effective Hamiltonian. This phenomenon originates from the interference of the dynamical phases and is very useful for applications in homodyne detection. These general results should be important and helpful for driven quantum TLS used in quantum information processing.

————

* xia-208@163.com
† yixx@nenu.edu.cn

[1] F. Grossmann, T. Dittrich, P. Jung, and P. Hänggi, "Coherent destruction of tunneling," Phys. Rev. Lett. **67**, 516–519 (1991).

[2] M. Grifoni and P. Hänggi, "Driven quantum tunneling," Phys. Rep. **304**, 229–354 (1998).

[3] H. W. Broer, I. Hoveijn, M. van Noort, C. Simó, and G. Vegter, "The parametrically forced pendulum: A case study in 1 1/2 degree of freedom," J. Dyn. Diff. Equat. **16**, 897–947 (2004).

[4] A. Das, "Exotic freezing of response in a quantum many-body system," Phys. Rev. B **82**, 172402 (2010).

[5] C. E. Creffield and G. Platero, "Coherent control of interacting particles using dynamical and Aharonov-Bohm phases," Phys. Rev. Lett. **105**, 086804 (2010).

[6] S. S. Hegde, H. Katiyar, T. S. Mahesh, and A. Das, "Freezing a quantum magnet by repeated quantum interference: An experimental realization," Phys. Rev. B **90**, 174407 (2014).

[7] T. Nag, D. Sen, and A. Dutta, "Maximum group velocity in a one-dimensional model with a sinusoidally varying staggered potential," Phys. Rev. A **91**, 063607 (2015).

[8] M. Bukov, L. D'Alessio, and A. Polkovnikov, "Universal high-frequency behavior of periodically driven systems: from dynamical stabilization to Floquet engineering," Adv. Phys. **64**, 139–226 (2015).

[9] A. Agarwala, U. Bhattacharya, A. Dutta, and D. Sen, "Effects of periodic kicking on dispersion and wave packet dynamics in graphene," Phys. Rev. B **93**, 174301 (2016).

[10] D. J. Luitz, A. Lazarides, and Y. Bar Lev, "Periodic and quasiperiodic revivals in periodically driven interacting quantum systems," Phys. Rev. B **97**, 020303 (2018).

[11] B. Horstmann, J. I. Cirac, and T. Roscilde, "Dynamics of localization phenomena for hard-core bosons in optical lattices," Phys. Rev. A **76**, 043625 (2007).

[12] C. M. Dai, W. Wang, and X. X. Yi, "Dynamical localization-delocalization crossover in the Aubry-André-Harper model," Phys. Rev. A **98**, 013635 (2018).

[13] S. Choi, D. A. Abanin, and M. D. Lukin, "Dynamically induced many-body localization," Phys. Rev. B **97**, 100301 (2018).

[14] D. Gagnon, F. Fillion-Gourdeau, J. Dumont, C. Lefebvre, and S. MacLean, "Suppression of multiphoton resonances in driven quantum systems via pulse shape optimization," Phys. Rev. Lett. **119**, 053203 (2017).

[15] G. S. Paraoanu, "Microwave-induced coupling of superconducting qubits," Phys. Rev. B **74**, 140504 (2006).

[16] C. E. Creffield, "Quantum control and entanglement using periodic driving fields," Phys. Rev. Lett. **99**, 110501 (2007).

[17] J. Li, K. Chalapat, and G. S. Paraoanu, "Entanglement of superconducting qubits via microwave fields: Classical and quantum regimes," Phys. Rev. B **78**, 064503 (2008).

[18] J. Li and G. S. Paraoanu, "Generation and propagation of entanglement in driven coupled-qubit systems," New J. Phys. **11**, 113020 (2009).

[19] Y. Song, J. P. Kestner, X. Wang, and S. Das Sarma, "Fast control of semiconductor qubits beyond the rotating-wave approximation," Phys. Rev. A **94**, 012321 (2016).

[20] Y.-C. Yang, S. N. Coppersmith, and M. Friesen, "High-fidelity single-qubit gates in a strongly driven quantum-dot hybrid qubit with $1/f$ charge noise," Phys. Rev. A **100**, 022337 (2019).

[21] A. Eckardt, C. Weiss, and M. Holthaus, "Superfluid-insulator transition in a periodically driven optical lattice," Phys. Rev. Lett. **95**, 260404 (2005).

[22] A. Eckardt, "Colloquium: Atomic quantum gases in periodically driven optical lattices," Rev. Mod. Phys. **89**, 011004 (2017).

[23] G. Sun and A. Eckardt, "Optimal frequency window for Floquet engineering in optical lattices," Phys. Rev. Research **2**, 013241 (2020).

[24] L. M. K. Vandersypen, H. Bluhm, J. S. Clarke, A. S. Dzurak, R. Ishihara, A. Morello, D. J. Reilly, L. R. Schreiber, and M. Veldhorst, "Interfacing spin qubits in quantum dots and donors—hot, dense, and coherent," npj Quantum Information **3**, 34 (2017).

[25] S. N. Shevchenko, S. Ashhab, and F. Nori, "Inverse Landau-Zener-Stückelberg problem for qubit-resonator systems," Phys. Rev. B **85**, 094502 (2012).

[26] M. F. Gonzalez-Zalba, S. N. Shevchenko, S. Barraud, J. R. Johansson, A. J. Ferguson, F. Nori, and A. C. Betz, "Gate-sensing coherent charge oscillations in a Silicon field-effect transistor," Nano Lett. **16**, 1614–1619 (2016).

[27] A. Chatterjee, S. N. Shevchenko, S. Barraud, R. M. Otxoa, F. Nori, John J. L. Morton, and M. F. Gonzalez-Zalba, "A silicon-based single-electron interferometer coupled to a fermionic sea," Phys. Rev. B **97**, 045405 (2018).

[28] R. M. Otxoa, A. Chatterjee, S. N. Shevchenko, S. Barraud, F. Nori, and M. F. Gonzalez-Zalba, "Quantum interference capacitor based on double-passage Landau-Zener-Stückelberg-Majorana interferometry," Phys. Rev. B **100**, 205425 (2019).

[29] P. Y. Wen, O. V. Ivakhnenko, M. A. Nakonechnyi, B. Suri, J.-J. Lin, W.-J. Lin, J. C. Chen, S. N. Shevchenko, F. Nori, and I.-C. Hoi, "Landau-Zener-Stückelberg-Majorana interferometry of a superconducting qubit in front of a mirror," Phys. Rev. B **102**, 075448 (2020).

[30] L. D. Landau, Phys. Z. Sowjetunion **2**, 46 (1932).

[31] C. Zener, Proc. R. Soc. Lond. A **137**, 696 (1932).

[32] N. Goldman and J. Dalibard, "Periodically driven quantum systems: Effective Hamiltonians and engineered gauge fields," Phys. Rev. X **4**, 031027 (2014).

[33] S. Rahav, I. Gilary, and S. Fishman, "Effective Hamiltonians for periodically driven systems," Phys. Rev. A **68**, 013820 (2003).

[34] K. Ono, S. N. Shevchenko, T. Mori, S. Moriyama, and F. Nori, "Quantum interferometry with a g-factor-tunable spin qubit," Phys. Rev. Lett. **122**, 207703 (2019).

[35] S. Savel'ev and F. Nori, "Experimentally realizable devices for controlling the motion of magnetic flux quanta in anisotropic superconductors," Nat. Mater. **1**, 179–184 (2002).

[36] D. Cole, S. Bending, S. Savel'ev, A. Grigorenko, T. Tamegai, and F. Nori, "Ratchet without spatial asymmetry for controlling the motion of magnetic flux quanta using time-asymmetric drives," Nat. Mater. **5**, 305–311 (2006).

[37] S. Savel'ev, F. Marchesoni, P. Hänggi, and F. Nori, "Transport via nonlinear signal mixing in ratchet devices," Phys. Rev. E **70**, 066109 (2004).

[38] A. Tonomura, "Conveyor belts for magnetic flux quanta," Nat. Mater. **5**, 257–258 (2006).

[39] N. Goldman, J. Dalibard, M. Aidelsburger, and N. R. Cooper, "Periodically driven quantum matter: The case of resonant modulations," Phys. Rev. A **91**, 033632 (2015).

[40] S.N. Shevchenko, S. Ashhab, and Franco Nori, "Landau–Zener–Stückelberg interferometry," Physics Reports **492**, 1–30 (2010).

[41] D. Gagnon, F. Fillion-Gourdeau, J. Dumont, C. Lefebvre, and S. MacLean, "Driven quantum tunneling and pair creation with graphene Landau levels," Phys. Rev. B **93**, 205415 (2016).

[42] F. Fillion-Gourdeau, D. Gagnon, C. Lefebvre, and S. MacLean, "Time-domain quantum interference in graphene," Phys. Rev. B **94**, 125423 (2016).

[43] M. O. Scully and M. S. Zubairy, Quantum Optics (Cambridge University Press, 1997).

[44] S.-K. Son, S. Han, and S.-I Chu, "Floquet formulation for the investigation of multiphoton quantum interference in a superconducting qubit driven by a strong ac field," Phys. Rev. A **79**, 032301 (2009).

[45] J. Pan, H. Z. Jooya, G. Sun, Y. Fan, P. Wu, D. A. Telnov, S.-I Chu, and S. Han, "Absorption spectra of superconducting qubits driven by bichromatic microwave fields," Phys. Rev. B **96**, 174518 (2017).

[46] J. H. Shirley, "Solution of the Schrödinger equation with a Hamiltonian periodic in time," Phys. Rev. **138**, B979–B987 (1965).

[47] H. Sambe, "Steady states and quasienergies of a quantum-mechanical system in an oscillating field," Phys. Rev. A **7**, 2203–2213 (1973).

[48] G. D. Fuchs, V. V. Dobrovitski, D. M. Toyli, F. J. Heremans, and D. D. Awschalom, "Gigahertz dynamics of a strongly driven single quantum spin," Science **326**, 1520–1522 (2009).

[49] M. P. Silveri, J. A. Tuorila, E. V. Thuneberg, and G. S. Paraoanu, "Quantum systems under frequency modulation," Rep. Prog. Phys. **80**, 056002 (2017).

[50] N. Lambert, M. Cirio, M. Delbecq, G. Allison, M. Marx, S. Tarucha, and F. Nori, "Amplified and tunable transverse and longitudinal spin-photon coupling in hybrid circuit-QED," Phys. Rev. B **97**, 125429 (2018).

[51] S. N. Shevchenko, A. I. Ryzhov, and F. Nori, "Low-frequency spectroscopy for quantum multilevel systems," Phys. Rev. B **98**, 195434 (2018).

[52] S. Basak, Y. Chougale, and R. Nath, "Periodically driven array of single Rydberg atoms," Phys. Rev. Lett. **120**, 123204 (2018).

[53] See the Supplemental Material at http://xxx which includes Refs. [32, 33], for further details of our calculations and simulations.

[54] S. Ashhab, J. R. Johansson, A. M. Zagoskin, and F. Nori, "Two-level systems driven by large-amplitude fields," Phys. Rev. A **75**, 063414 (2007).

[55] Jani Tuorila, Matti Silveri, Mika Sillanpää, Erkki Thuneberg, Yuriy Makhlin, and Pertti Hakonen, "Stark

effect and generalized bloch-siegert shift in a strongly driven two-level system," Phys. Rev. Lett. **105**, 257003 (2010).

[56] P. Neilinger, S. N. Shevchenko, J. Bogár, M. Rehák, G. Oelsner, D. S. Karpov, U. Hübner, O. Astafiev, M. Grajcar, and E. Il'ichev, "Landau-Zener-Stückelberg-Majorana lasing in circuit quantum electrodynamics," Phys. Rev. B **94**, 094519 (2016).

[57] M. P. Silveri, K. S. Kumar, J. Tuorila, J. Li, A. Vepsäläinen, E. V. Thuneberg, and G. S. Paraoanu, "Stückelberg interference in a superconducting qubit under periodic latching modulation," New Journal of Physics **17**, 043058 (2015).

[58] O. V. Ivakhnenko, S. N. Shevchenko, and F. Nori, "Simulating quantum dynamical phenomena using classical oscillators: Landau-Zener-Stückelberg-Majorana interferometry, latching modulation, and motional averaging," Sci. Rep. **8**, 12218 (2018).

Supplementary Material for "Coherent Control of Two-level Systems with Periodic N-Steps Driving Fields"

In this supplementary material, we first present the detailed derivation process for the solution of the dynamical equation in periodic N-steps driven two-level system. Since the solution is a set of quasi-periodic functions, one can rewrite the solution as the superposition of cosine functions. Then, by the Fourier transform, we obtain the frequencies, the amplitudes, and the phases for each cosine function. Thirdly, although we have given the exact solutions of transition probability, the expression is too cumbersome for a set of general parameters. Thus we empirically provide a modified formula for the transition probability in the two-steps sequence and testify the validity by numerical simulations. Fourthly, we present the derivation process for the expressions of physical parameters when we presuppose that the transition probability exhibits the beat phenomena, and the results show the waveforms are intricate and singular. Finally, we demonstrate that the beat phenomena always exist in periodic N-steps driven system, and how to empirically obtain the expressions of the frequencies ϖ_1 and ϖ_1' in the beating formula.

Note that the parameters and operators in this supplementary material are defined to be the same as those in the main text.

Solutions for the dynamical equation in periodic N-steps driven two-level systems

The physical model we consider here is a two-level system (TLS) driven by the periodic N-steps driving field. The general form of its Hamiltonian reads ($\hbar = 1$)

$$H(t) = \sum_{k=0}^{\mathcal{N}} \sum_{n=1}^{N} H_n \left[\zeta \left(t - kT - \sum_{m=0}^{n-1} \tau_m \right) - \zeta \left(t - kT - \sum_{m=0}^{n} \tau_m \right) \right], \tag{9}$$

where $H_n = \Delta_n |2\rangle\langle 2| + \epsilon_n \exp(i\theta_n)|1\rangle\langle 2| + \text{H.c.}$, $\zeta(t)$ is the Heaviside function, $\tau_0 = 0$, τ_n ($n = 1, ..., N$) is the interaction time between TLS and the n-th step driving field, and $T = \tau_N + \tau_{N-1} + \cdots + \tau_1$ is the period of the N-steps sequence.

Generally speaking, the evolution operator of periodically driven systems can be divided into two parts:

$$\mathbb{U}(t) = \mathbb{P}(t) \exp(-iH_{\text{eff}}t), \tag{10}$$

where the unitary operator $\mathbb{P}(t)$ has the same period as the system Hamiltonian. The eigenvalues of the effective Hamiltonian H_{eff} are referred to as the quasienergies of the system. Different from both this partitioning and the partition introduced in Refs. [32, 33], we directly divide the evolution operator of a periodic N-steps driven system at arbitrary final time $t_f = t + \mathcal{N}T$ ($t < T$, $\mathcal{N} = 1, 2, ...$) into two parts:

$$\mathbb{U}(t_f) = \mathbb{U}(t) \underbrace{\mathbb{U}(T) \cdots \mathbb{U}(T)}_{\mathcal{N}} = \mathbb{U}(t)\mathbb{U}(\mathcal{N}T) \equiv \exp[-i\mathcal{M}(t)] \exp(-iH_{\text{eff}}\mathcal{N}T), \tag{11}$$

where $\mathbb{U}(T) = U_N(\tau_N)U_{N-1}(\tau_{N-1}) \cdots U_1(\tau_1) \equiv \exp(-iH_{\text{eff}}T)$ is the evolution operator within one period. $U_n(t) = \exp(-iH_n t)$ represents the evolution operator for the nth Hamiltonian, where $n = 1, ..., N$. Physically, the time-dependent micromotion operator $\mathcal{M}(t)$ describes the short time-scale ("fast" part) dynamics of the system, and the time-independent effective Hamiltonian H_{eff} describes the long time-scale ("slow" part) dynamics of the system.

In order to derive the expression of evolution operator $\mathbb{U}(t_f)$ for the periodic N-steps driven system, we need to calculate both the micromotion operator $\mathcal{M}(t)$ and the effective Hamiltonian H_{eff}. To be specific, the micromotion operator $\mathcal{M}(t) = \Delta_{\mathcal{M}}(t)|2\rangle\langle 2| + \epsilon_{\mathcal{M}}(t)\exp[i\theta_{\mathcal{M}}(t)]|1\rangle\langle 2| + \text{H.c.}$ is defined by the evolution operator $\mathbb{U}(t)$, which reads

$$\exp[-i\mathcal{M}(t)] \equiv \mathbb{U}(t) = \begin{cases} U_1(t), & t \in [0, \tau_1], \\ U_2(t-\tau_1)U_1(\tau_1), & t \in (\tau_1, \tau_2 + \tau_1], \\ U_3(t-\tau_2-\tau_1)U_2(\tau_2)U_1(\tau_1), & t \in (\tau_2 + \tau_1, \tau_3 + \tau_2 + \tau_1], \\ \cdots & \cdots \\ U_N(t - \sum_{k=1}^{N-1}\tau_k)U_{N-1}(\tau_{N-1})\cdots U_2(\tau_2)U_1(\tau_1), & t \in (\sum_{k=1}^{N-1}\tau_k, \sum_{k=1}^{N}\tau_k], \end{cases} \tag{12}$$

where $U_n(t) = \exp(-iH_n t)$.

When $t \in [0, \tau_1]$, the expression of the evolution operator becomes

$$\mathbb{U}(t) = U_1(t) = \begin{bmatrix} \cos(E_1 t) + i\frac{\Delta_1}{2E_1}\sin(E_1 t) & -i\frac{\epsilon_1 e^{i\theta_1}}{E_1}\sin(E_1 t) \\ -i\frac{\epsilon_1 e^{-i\theta_1}}{E_1}\sin(E_1 t) & \cos(E_1 t) - i\frac{\Delta_1}{2E_1}\sin(E_1 t) \end{bmatrix} = \begin{bmatrix} A_1(t) + iB_1(t) & C_1(t) - iD_1(t) \\ -C_1(t) - iD_1(t) & A_1(t) - iB_1(t) \end{bmatrix}. \tag{13}$$

Comparing the left-hand side and the right-hand side of Eq. (13), we find

$$A_1(t) = \cos(E_1 t), \qquad B_1(t) = \frac{\Delta_1}{2E_1} \sin(E_1 t), \qquad C_1(t) = \frac{\epsilon_1 \sin\theta_1}{E_1} \sin(E_1 t), \qquad D_1(t) = \frac{\epsilon_1 \cos\theta_1}{E_1} \sin(E_1 t),$$

where $E_1 = \sqrt{\epsilon_1^2 + \Delta_1^2/4}$. Then, by inversely solving the equation $\exp[-i\mathcal{M}(t)] = \mathbb{U}(t)$, we have

$$\Delta_\mathcal{M}(t) = \frac{2B_1(t)}{\sqrt{1 - A_1(t)^2}} \arccos A_1(t), \qquad \epsilon_\mathcal{M}(t) = \frac{\sqrt{C_1(t)^2 + D_1(t)^2}}{\sqrt{1 - A_1(t)^2}} \arccos A_1(t), \qquad \theta_\mathcal{M}(t) = \arctan \frac{C_1(t)}{D_1(t)}.$$

Similarly, when $t \in (\tau_1, \tau_2 + \tau_1]$, the expression of the evolution operator reads

$$
\begin{aligned}
\mathbb{U}(t) &= U_2(t - \tau_1)U_1(\tau_1) = \exp[-iH_2(t - \tau_1)]\exp(-iH_1\tau_1) \\
&= \begin{bmatrix} \cos E_2(t - \tau_1) + i\dfrac{\Delta_2}{2E_2}\sin E_2(t - \tau_1) & -i\dfrac{\epsilon_2 e^{i\theta_2}}{E_2}\sin E_2(t - \tau_1) \\[2mm] -i\dfrac{\epsilon_2 e^{-i\theta_2}}{E_2}\sin E_2(t - \tau_1) & \cos E_2(t - \tau_1) - i\dfrac{\Delta_2}{2E_2}\sin E_2(t - \tau_1) \end{bmatrix} \begin{bmatrix} A_1(\tau_1) + iB_1(\tau_1) & C_1(\tau_1) - iD_1(\tau_1) \\ -C_1(\tau_1) - iD_1(\tau_1) & A_1(\tau_1) - iB_1(\tau_1) \end{bmatrix} \\[2mm]
&= \begin{bmatrix} A_2(t) + iB_2(t) & C_2(t) - iD_2(t) \\ -C_2(t) - iD_2(t) & A_2(t) - iB_2(t) \end{bmatrix}.
\end{aligned}
\tag{14}
$$

According to Eq. (14), we obtain the coefficients $A_2(t)$, $B_2(t)$, $C_2(t)$, and $D_2(t)$

$$A_2(t) = \cos E_1\tau_1 \cos E_2(t - \tau_1) - \frac{\Delta_1\Delta_2 + 4\epsilon_1\epsilon_2 \cos(\theta_1 - \theta_2)}{4E_1 E_2} \sin E_1\tau_1 \sin E_2(t - \tau_1),$$

$$B_2(t) = \frac{\Delta_1}{2E_1} \sin E_1\tau_1 \cos E_2(t - \tau_1) + \left[\frac{\Delta_2}{2E_2} \cos E_1\tau_1 + \frac{\epsilon_1\epsilon_2 \sin(\theta_1 - \theta_2)}{E_1 E_2} \sin E_1\tau_1\right] \sin E_2(t - \tau_1),$$

$$C_2(t) = \frac{\epsilon_1 \sin\theta_1}{E_1} \sin E_1\tau_1 \cos E_2(t - \tau_1) + \left(\frac{\epsilon_2 \sin\theta_2}{E_2} \cos E_1\tau_1 + \frac{\Delta_1\epsilon_2 \cos\theta_2 - \Delta_2\epsilon_1 \cos\theta_1}{2E_1 E_2} \sin E_1\tau_1\right) \sin E_2(t - \tau_1),$$

$$D_2(t) = \frac{\epsilon_1 \cos\theta_1}{E_1} \sin E_1\tau_1 \cos E_2(t - \tau_1) + \left(\frac{\epsilon_2 \cos\theta_2}{E_2} \cos E_1\tau_1 + \frac{\Delta_1\epsilon_2 \sin\theta_2 - \Delta_2\epsilon_1 \sin\theta_1}{2E_1 E_2} \sin E_1\tau_1\right) \sin E_2(t - \tau_1).$$

As a result, we have

$$\Delta_\mathcal{M}(t) = \frac{2B_2(t)}{\sqrt{1 - A_2(t)^2}} \arccos A_2(t), \qquad \epsilon_\mathcal{M}(t) = \frac{\sqrt{C_2(t)^2 + D_2(t)^2}}{\sqrt{1 - A_2(t)^2}} \arccos A_2(t), \qquad \theta_\mathcal{M}(t) = \arctan \frac{C_2(t)}{D_2(t)}.$$

It is easily found from Eqs. (13)-(14) that the matrix $\mathbb{U}(t)$ has definite symmetry: the real (imaginary) part of the diagonal (off-diagonal) elements is identical, while the imaginary (real) part of the diagonal (off-diagonal) elements are opposite. Thus, we can assume in advance that the form of the evolution operator $\mathbb{U}(t')$ after $(n-1)$-steps sequence can be written as

$$
\begin{aligned}
\mathbb{U}(t') &= U_{n-1}(\tau_{n-1}) \cdots U_2(\tau_2)U_1(\tau_1) \\
&= \begin{bmatrix} A_{n-1}(t') + iB_{n-1}(t') & C_{n-1}(t') - iD_{n-1}(t') \\ -C_{n-1}(t') - iD_{n-1}(t') & A_{n-1}(t') - iB_{n-1}(t') \end{bmatrix},
\end{aligned}
\tag{15}
$$

where $t' = \sum_{k=1}^{n-1} \tau_k$. When $0 < (t - t') < \tau_n$, the form of the evolution operator $\mathbb{U}(t)$ is

$$
\begin{aligned}
\mathbb{U}(t) &= U_n(t - t')\mathbb{U}(t') \\
&= \begin{bmatrix} \cos E_n(t - t') + i\dfrac{\Delta_n}{2E_n}\sin E_n(t - t') & -i\dfrac{\epsilon_n e^{i\theta_n}}{E_n}\sin E_n(t - t') \\[2mm] -i\dfrac{\epsilon_n e^{-i\theta_n}}{E_n}\sin E_n(t - t') & \cos E_n(t - t') - i\dfrac{\Delta_n}{2E_n}\sin E_n(t - t') \end{bmatrix} \\[2mm]
&\quad \cdot \begin{bmatrix} A_{n-1}(t') + iB_{n-1}(t') & C_{n-1}(t') - iD_{n-1}(t') \\ -C_{n-1}(t') - iD_{n-1}(t') & A_{n-1}(t') - iB_{n-1}(t') \end{bmatrix} \\[2mm]
&= \begin{bmatrix} A_n(t) + iB_n(t) & C_n(t) - iD_n(t) \\ -C_n(t) - iD_n(t) & A_n(t) - iB_n(t) \end{bmatrix}.
\end{aligned}
\tag{16}
$$

According to Eq. (16), we obtain the following recursive equations for the coefficients $A_n(t)$, $B_n(t)$, $C_n(t)$, and $D_n(t)$:

$$A_n(t) = A_{n-1}(t') \cos E_n(t - t') - [\mathcal{A}_{n-1}(t') \cdot \mathcal{E}_n] \sin E_n(t - t'),$$

$$B_n(t) = B_{n-1}(t') \cos E_n(t - t') + [\mathcal{B}_{n-1}(t') \cdot \mathcal{E}_n] \sin E_n(t - t'),$$

$$C_n(t) = C_{n-1}(t') \cos E_n(t - t') + [\mathcal{C}_{n-1}(t') \cdot \mathcal{E}_n] \sin E_n(t - t'),$$

$$D_n(t) = D_{n-1}(t') \cos E_n(t - t') + [\mathcal{D}_{n-1}(t') \cdot \mathcal{E}_n] \sin E_n(t - t'), \tag{17}$$

where the vectors are

$$\mathcal{A}_{n-1}(t) = (D_{n-1}(t), C_{n-1}(t), B_{n-1}(t)),$$

$$\mathcal{B}_{n-1}(t) = (C_{n-1}(t), -D_{n-1}(t), A_{n-1}(t)),$$

$$\mathcal{C}_{n-1}(t) = (-B_{n-1}(t), A_{n-1}(t), D_{n-1}(t)),$$

$$\mathcal{D}_{n-1}(t) = (A_{n-1}(t), B_{n-1}(t), -C_{n-1}(t)),$$

$$\mathcal{E}_n = (\epsilon_n \cos\theta_n, \epsilon_n \sin\theta_n, \Delta_n/2)/E_n,$$

and $E_n = \sqrt{\epsilon_n^2 + \Delta_n^2/4}$. As a result, we have

$$\Delta_{\mathcal{M}}(t) = \frac{2B_n(t)}{\sqrt{1 - A_n(t)^2}} \arccos A_n(t), \quad \epsilon_{\mathcal{M}}(t) = \frac{\sqrt{C_n(t)^2 + D_n(t)^2}}{\sqrt{1 - A_n(t)^2}} \arccos A_n(t), \quad \theta_{\mathcal{M}}(t) = \arctan \frac{C_n(t)}{D_n(t)}. \tag{18}$$

This is the exact solutions for the micromotion operator $\mathcal{M}(t)$ when $t' < t < \tau_n + t'$, $n = 1, ..., N - 1$.

To derive the expression of the effective Hamiltonian, we need to exploit the primitive definition $\mathbb{U}(T) = U_N(\tau_N)U_{N-1}(\tau_{N-1}) \cdots U_2(\tau_2)U_1(\tau_1) \equiv \exp(-iH_{\text{eff}}T)$. Further observations indicate that the effective Hamiltonian H_{eff} is a special case of the micromotion operator $\mathcal{M}(t)$, and they satisfy the relation: $H_{\text{eff}} = \mathcal{M}(T)/T$. Therefore, the general form of the time-independent effective Hamiltonian H_{eff} for the periodic N-steps driven system reads

$$H_{\text{eff}} = \Delta_{\text{eff}} |2\rangle\langle2| + [\epsilon_{\text{eff}} \exp(i\theta_{\text{eff}})|1\rangle\langle2| + \text{H.c.}], \tag{19}$$

where the effective quantities are

$$\Delta_{\text{eff}} = \frac{2B_N(T)}{T\sqrt{1 - A_N(T)^2}} \arccos A_N(T), \quad \epsilon_{\text{eff}} = \frac{\sqrt{C_N(T)^2 + D_N(T)^2}}{T\sqrt{1 - A_N(T)^2}} \arccos A_N(T), \quad \theta_{\text{eff}} = \arctan \frac{C_N(T)}{D_N(T)}.$$

Note that the coefficient $A_N(T)$ should be positive when the transition probability $P_{1\rightarrow2}(t)$ from $|1\rangle$ to $|2\rangle$ in the time interval $[0, T]$ is less than $P_{1\rightarrow2}(\frac{\pi}{2E_{\text{eff}}})$, where $E_{\text{eff}} = \sqrt{\epsilon_{\text{eff}}^2 + \Delta_{\text{eff}}^2/4}$.

Now, we can calculate the evolution operator $\mathbb{U}(t_f)$, which reads

$$\mathbb{U}(t_f) = \mathbb{U}(t)\mathbb{U}(NT) = \begin{bmatrix} A_n(t) + iB_n(t) & C_n(t) - iD_n(t) \\ -C_n(t) - iD_n(t) & A_n(t) - iB_n(t) \end{bmatrix} \begin{bmatrix} A_N(T) + iB_N(T) & C_N(T) - iD_N(T) \\ -C_N(T) - iD_N(T) & A_N(T) - iB_N(T) \end{bmatrix}^{\mathcal{N}}$$

$$= \begin{bmatrix} A(t) + iB(t) & C(t) - iD(t) \\ -C(t) - iD(t) & A(t) - iB(t) \end{bmatrix}. \tag{20}$$

The coefficients $A(t)$, $B(t)$, $C(t)$, and $D(t)$ are given by

$$A(t) = A_n(t) \cos\mathcal{N}\Theta - [\mathcal{A}_n(t) \cdot \mathcal{A}_N^{\mathtt{T}}(T)] \frac{\sin\mathcal{N}\Theta}{\sin\Theta},$$

$$B(t) = B_n(t) \cos\mathcal{N}\Theta + [\mathcal{B}_n(t) \cdot \text{diag}\{-1, -1, 1\} \cdot \mathcal{A}_N^{\mathtt{T}}(T)] \frac{\sin\mathcal{N}\Theta}{\sin\Theta},$$

$$C(t) = C_n(t) \cos\mathcal{N}\Theta + [\mathcal{C}_n(t) \cdot \text{diag}\{-1, 1, -1\} \cdot \mathcal{A}_N^{\mathtt{T}}(T)] \frac{\sin\mathcal{N}\Theta}{\sin\Theta},$$

$$D(t) = D_n(t) \cos\mathcal{N}\Theta + [\mathcal{D}_n(t) \cdot \text{diag}\{1, -1, -1\} \cdot \mathcal{A}_N^{\mathtt{T}}(T)] \frac{\sin\mathcal{N}\Theta}{\sin\Theta}. \tag{21}$$

where $\Theta = \arccos A_N(T)$ and the superscript $\mathtt{T}$ denotes transposition. It is worth mentioning that both the effective Hamiltonian in Eq. (19) and the evolution operator in Eq. (20) are exact, since we do not make any approximations in the derivation.

As an illustration, let us calculate the expression (17) for the two-steps sequence, where the Hamiltonian is

$$H(t) = \begin{cases} H_1 = \Delta_1|2\rangle\langle2| + \big[\epsilon_1\exp(i\theta_1)|1\rangle\langle2| + \text{H.c.}\big], & t \in [kT, \tau_1 + kT), \\ H_2 = \Delta_2|2\rangle\langle2| + \big[\epsilon_2\exp(i\theta_2)|1\rangle\langle2| + \text{H.c.}\big], & t \in [\tau_1 + kT, (k+1)T). \end{cases} \tag{22}$$

Here, the period is $T = \tau_1 + \tau_2$, and $k = 0, 1, ..., \mathcal{N}$. The coefficients $A_2(T)$, $B_2(T)$, $C_2(T)$, and $D_2(T)$ are

$$A_2(T) = \cos E_1\tau_1 \cos E_2\tau_2 - \frac{\Delta_1\Delta_2 + 4\epsilon_1\epsilon_2\cos(\theta_1 - \theta_2)}{4E_1E_2}\sin E_1\tau_1 \sin E_2\tau_2,$$

$$B_2(T) = \frac{\Delta_1}{2E_1}\sin E_1\tau_1 \cos E_2\tau_2 + \left[\frac{\Delta_2}{2E_2}\cos E_1\tau_1 + \frac{\epsilon_1\epsilon_2\sin(\theta_1 - \theta_2)}{E_1E_2}\sin E_1\tau_1\right]\sin E_2\tau_2,$$

$$C_2(T) = \frac{\epsilon_1\sin\theta_1}{E_1}\sin E_1\tau_1 \cos E_2\tau_2 + \left(\frac{\epsilon_2\sin\theta_2}{E_2}\cos E_1\tau_1 + \frac{\Delta_2\epsilon_1\cos\theta_1 - \Delta_1\epsilon_2\cos\theta_2}{2E_1E_2}\sin E_1\tau_1\right)\sin E_2\tau_2,$$

$$D_2(T) = \frac{\epsilon_1\cos\theta_1}{E_1}\sin E_1\tau_1 \cos E_2\tau_2 + \left(\frac{\epsilon_2\cos\theta_2}{E_2}\cos E_1\tau_1 + \frac{\Delta_1\epsilon_2\sin\theta_2 - \Delta_2\epsilon_1\sin\theta_1}{2E_1E_2}\sin E_1\tau_1\right)\sin E_2\tau_2. \tag{23}$$

Thus, the effective Hamiltonian H_{eff} for the two-steps sequence becomes

$$H_{\text{eff}} = \Delta_{\text{eff}}|2\rangle\langle2| + \big[\epsilon_{\text{eff}}\exp(i\theta_{\text{eff}})|1\rangle\langle2| + \text{H.c.}\big], \tag{24}$$

where the effective quantities are

$$\Delta_{\text{eff}} = \frac{2B_2(T)}{T\sqrt{1 - A_2(T)^2}}\arccos A_2(T), \qquad \epsilon_{\text{eff}} = \frac{\sqrt{C_2(T)^2 + D_2(T)^2}}{T\sqrt{1 - A_2(T)^2}}\arccos A_2(T), \qquad \theta_{\text{eff}} = \arctan\frac{C_2(T)}{D_2(T)}.$$

For the two-steps sequence with one jump, the coefficients $A_3(T)$, $B_3(T)$, $C_3(T)$, and $D_3(T)$ are

$$A_3(T) = \cos E_1\tau_1 \cos E_2\tau_2 - \frac{\Delta_1\Delta_2 + 4\epsilon_1\epsilon_2\cos(\theta_1 - \theta_2)}{4E_1E_2}\sin E_1\tau_1 \sin E_2\tau_2,$$

$$B_3(T) = \frac{\Delta_1}{2E_1}\sin E_1\tau_1 \cos E_2\tau_2 + \frac{\Delta_2}{2E_2}\cos E_1\tau_1 \sin E_2\tau_2 + \frac{\epsilon_1\epsilon_2\sin(\theta_1 - \theta_2)}{E_1E_2}\sin[(2\lambda - 1)E_1\tau_1]\sin E_2\tau_2$$
$$+ \frac{\Delta_2\epsilon_1^2 - \Delta_1\epsilon_1\epsilon_2}{E_1^2E_2}\sin[(1 - \lambda)E_1\tau_1]\sin\lambda E_1\tau_1 \sin E_2\tau_2$$

$$C_3(T) = \frac{\epsilon_1\sin\theta_1}{E_1}\sin E_1\tau_1 \cos E_2\tau_2 + \frac{\epsilon_2\sin\theta_2}{E_2}\cos[(1 - \lambda)E_1\tau_1]\cos\lambda E_1\tau_1 \sin E_2\tau_2$$
$$+ \frac{\Delta_2\epsilon_1\cos\theta_1 - \Delta_1\epsilon_2\cos\theta_2}{2E_1E_2}\sin[(2\lambda - 1)E_1\tau_1]\sin E_2\tau_2$$
$$+ \frac{\Delta_1^2\epsilon_2\sin\theta_2 - 2\epsilon_1\Delta_1\Delta_2\sin\theta_1 + 4\epsilon_1^2\epsilon_2\sin(2\theta_1 - \theta_2)}{4E_1^2E_2}\sin[(1 - \lambda)E_1\tau_1]\sin\lambda E_1\tau_1 \sin E_2\tau_2,$$

$$D_3(T) = \frac{\epsilon_1\cos\theta_1}{E_1}\sin E_1\tau_1 \cos E_2\tau_2 + \frac{\epsilon_2\cos\theta_2}{E_2}\cos[(1 - \lambda)E_1\tau_1]\cos\lambda E_1\tau_1 \sin E_2\tau_2$$
$$+ \frac{\Delta_1\epsilon_2\sin\theta_2 - \Delta_2\epsilon_1\sin\theta_1}{2E_1E_2}\sin[(2\lambda - 1)E_1\tau_1]\sin E_2\tau_2$$
$$+ \frac{\Delta_1^2\epsilon_2\cos\theta_2 - 2\epsilon_1\Delta_1\Delta_2\cos\theta_1 + 4\epsilon_1^2\epsilon_2\cos(2\theta_1 - \theta_2)}{4E_1^2E_2}\sin[(1 - \lambda)E_1\tau_1]\sin\lambda E_1\tau_1 \sin E_2\tau_2. \tag{25}$$

Thus, the effective Hamiltonian H_{eff} for the two-steps sequence with one jump becomes

$$H_{\text{eff}}(\lambda) = \Delta_{\text{eff}}|2\rangle\langle2| + \big[\epsilon_{\text{eff}}\exp(i\theta_{\text{eff}})|1\rangle\langle2| + \text{H.c.}\big], \tag{26}$$

where the effective quantities are

$$\Delta_{\text{eff}} = \frac{2B_3(T)}{T\sqrt{1 - A_3(T)^2}}\arccos A_3(T), \qquad \epsilon_{\text{eff}} = \frac{\sqrt{C_3(T)^2 + D_3(T)^2}}{T\sqrt{1 - A_3(T)^2}}\arccos A_3(T), \qquad \theta_{\text{eff}} = \arctan\frac{C_3(T)}{D_3(T)}.$$

Furthermore, one can easily achieve the expression of the time-dependent transition probability $P_{1\to2}(t)$ from $|1\rangle$ to $|2\rangle$, which is

$$P_{1\to2}(t) = C(t)^2 + D(t)^2. \tag{27}$$

According to Eq. (21), the expressions of $C(t)$ and $D(t)$ can be written as

$$C(t) = \begin{cases} R_k^{1c} \cos E_1 t + R_k^{1s} \sin E_1 t, & t \in [kT, \tau_1 + kT), \\ Q_k^{1c} \cos E_2(t - \tau_1) + Q_k^{1s} \sin E_2(t - \tau_1), & t \in [\tau_1 + kT, (k+1)T), \end{cases}$$

$$D(t) = \begin{cases} R_k^{2c} \cos E_1 t + R_k^{2s} \sin E_1 t, & t \in [kT, \tau_1 + kT), \\ Q_k^{2c} \cos E_2(t - \tau_1) + Q_k^{2s} \sin E_2(t - \tau_1), & t \in [\tau_1 + kT, (k+1)T), \end{cases} \qquad (28)$$

where the time-independent coefficients are

$$R_k^{1c} = C_2(T) \frac{\sin k\Theta}{\sin \Theta},$$

$$R_k^{1s} = (-B_2(T) \frac{\sin k\Theta}{\sin \Theta}, \cos k\Theta, D_2(T) \frac{\sin k\Theta}{\sin \Theta}) \cdot \mathcal{E}_1,$$

$$Q_k^{1c} = C_1(\tau_1) \cos k\Theta + \left[\mathcal{C}_1(\tau_1) \cdot \mathrm{diag}\{-1, 1, -1\} \cdot \mathcal{A}_2^\mathsf{T}(T) \right] \frac{\sin k\Theta}{\sin \Theta},$$

$$Q_k^{1s} = [\mathcal{C}_1(\tau_1) \cdot \mathcal{E}_2] \cos k\Theta + \left\{ D_2(T) [\mathcal{B}_1(\tau_1) \cdot \mathcal{E}_2] - C_2(T) [\mathcal{A}_1(\tau_1) \cdot \mathcal{E}_2] - B_2(T) [\mathcal{D}_1(\tau_1) \cdot \mathcal{E}_2] \right\} \frac{\sin k\Theta}{\sin \Theta},$$

$$R_k^{2c} = D_2(T) \frac{\sin k\Theta}{\sin \Theta},$$

$$R_k^{2s} = (\cos k\Theta, B_2(T) \frac{\sin k\Theta}{\sin \Theta}, -C_2(T) \frac{\sin k\Theta}{\sin \Theta}) \cdot \mathcal{E}_1,$$

$$Q_k^{2c} = D_1(\tau_1) \cos k\Theta + \left[\mathcal{D}_1(\tau_1) \cdot \mathrm{diag}\{1, -1, -1\} \cdot \mathcal{A}_2^\mathsf{T}(T) \right] \frac{\sin k\Theta}{\sin \Theta},$$

$$Q_k^{2s} = [\mathcal{D}_1(\tau_1) \cdot \mathcal{E}_2] \cos k\Theta - \left\{ D_2(T) [\mathcal{A}_1(\tau_1) \cdot \mathcal{E}_2] + C_2(T) [\mathcal{B}_1(\tau_1) \cdot \mathcal{E}_2] - B_2(T) [\mathcal{C}_1(\tau_1) \cdot \mathcal{E}_2] \right\} \frac{\sin k\Theta}{\sin \Theta},$$

As a result, the exact solution of time-dependent transition probability $P_{1\to 2}(t)$ from $|1\rangle$ to $|2\rangle$ becomes

$$P_{1\to 2}(t) = C(t)^2 + D(t)^2 = \begin{cases} R_k^0 + R_k^c \cos 2E_1 t + R_k^s \sin 2E_1 t, & t \in [kT, \tau_1 + kT), \\ Q_k^0 + Q_k^c \cos 2E_2(t - \tau_1) + Q_k^s \sin 2E_2(t - \tau_1), & t \in [\tau_1 + kT, (k+1)T), \end{cases} \qquad (29)$$

where the coefficients are

$$R_k^0 = \frac{(R_k^{1c})^2 + (R_k^{1s})^2 + (R_k^{2c})^2 + (R_k^{2s})^2}{2}, \quad R_k^c = \frac{(R_k^{1c})^2 - (R_k^{1s})^2 + (R_k^{2c})^2 - (R_k^{2s})^2}{2}, \quad R_k^s = R_k^{1c} R_k^{1s} + R_k^{2c} R_k^{2s},$$

$$Q_k^0 = \frac{(Q_k^{1c})^2 + (Q_k^{1s})^2 + (Q_k^{2c})^2 + (Q_k^{2s})^2}{2}, \quad Q_k^c = \frac{(Q_k^{1c})^2 - (Q_k^{1s})^2 + (Q_k^{2c})^2 - (Q_k^{2s})^2}{2}, \quad Q_k^s = Q_k^{1c} Q_k^{1s} + Q_k^{2c} Q_k^{2s}.$$

Fourier transform of the time-dependent transition probability $P_{1\to 2}(t)$

In this section, we consider a two-steps sequence as an example to demonstrate the Fourier transform of the time-dependent transition probability $P_{1\to 2}(t)$. Note that it is easily generalized to the case of $N > 2$.

Although $P_{1\to 2}(t)$ in Eq. (29) is a quasi-periodic function rather than a periodic function, the frequency spectrum is still discrete and the base frequency is $\omega_T = 2\pi/T$. Moreover, the frequency spectrum is also associated with the effective Rabi frequency $\omega_{\mathrm{eff}} = \sqrt{\epsilon_{\mathrm{eff}}^2 + \Delta_{\mathrm{eff}}^2/4}$. By Fourier transform, the expression of $P_{1\to 2}(t)$ can be expanded in terms of cosine functions,

$$P_{1\to 2}(t) = \bar{b} + \sum_{l=-\infty}^{\infty} \left\{ b_l \cos \left[(2\omega_{\mathrm{eff}} + l\omega_T)t - \varphi_l \right] + b_l' \cos \left[(l+1)\omega_T t - \varphi_l' \right] \right\}, \qquad (30)$$

where $b_l = \sqrt{(c_l)^2 + (d_l)^2}$, $b_l' = \sqrt{(c_l')^2 + (d_l')^2}$, $\varphi_l = \arctan[c_l/d_l]$, $\varphi_l' = \arctan[c_l'/d_l']$, and the coefficients read

$$\bar{b} = \lim_{K \to \infty} \frac{1}{KT} \int_0^{KT} P_{1\to 2}(t) dt,$$

$$c_l = \lim_{K \to \infty} \frac{2}{KT} \int_0^{KT} P_{1\to 2}(t) \sin(2\omega_{\mathrm{eff}} + l\omega_T) t \, dt,$$

$$d_l = \lim_{K \to \infty} \frac{2}{KT} \int_0^{KT} P_{1 \to 2}(t) \cos(2\omega_{\text{eff}} + l\omega_T) t \, dt,$$

$$c_l' = \lim_{K \to \infty} \frac{2}{KT} \int_0^{KT} P_{1 \to 2}(t) \sin(l+1)\omega_T t \, dt,$$

$$d_l' = \lim_{K \to \infty} \frac{2}{KT} \int_0^{KT} P_{1 \to 2}(t) \cos(l+1)\omega_T t \, dt.$$

In order to derive those coefficients, it is instructive to calculate the following integrals:

$$I_l(t_2, t_1, R^c, R^s, \omega_{\text{eff}}, \tau_1) \equiv \int_{t_1}^{t_2} \left[R^c \cos(2\omega_{\text{eff}} + l\omega_T)(t - \tau_1) + R^s \sin(2\omega_{\text{eff}} + l\omega_T)(t - \tau_1) \right] dt$$

$$= \frac{R^c}{2\omega_{\text{eff}} + l\omega_T} \left[\sin(2\omega_{\text{eff}} + l\omega_T)(t_2 - \tau_1) - \sin(2\omega_{\text{eff}} + l\omega_T)(t_1 - \tau_1) \right]$$

$$- \frac{R^s}{2\omega_{\text{eff}} + l\omega_T} \left[\cos(2\omega_{\text{eff}} + l\omega_T)(t_2 - \tau_1) - \cos(2\omega_{\text{eff}} + l\omega_T)(t_1 - \tau_1) \right],$$

$$I_l^c(t_2, t_1, R^c, R^s, \omega_{\text{eff}}, E_2, \tau_1) \equiv \int_{t_1}^{t_2} \left[R^c \cos 2E_2(t - \tau_1) + R^s \sin 2E_2(t - \tau_1) \right] \cos(2\omega_{\text{eff}} + l\omega_T) t \, dt$$

$$= R^c \frac{\sin[(2\omega_{\text{eff}} + l\omega_T + 2E_2)t_2 - 2E_2\tau_1] - \sin[(2\omega_{\text{eff}} + l\omega_T + 2E_2)t_1 - 2E_2\tau_1]}{2(2\omega_{\text{eff}} + l\omega_T + 2E_2)}$$

$$+ R^c \frac{\sin[(2\omega_{\text{eff}} + l\omega_T - 2E_2)t_2 + 2E_2\tau_1] - \sin[(2\omega_{\text{eff}} + l\omega_T - 2E_2)t_1 + 2E_2\tau_1]}{2(2\omega_{\text{eff}} + l\omega_T - 2E_2)}$$

$$+ R^s \frac{\cos[(2\omega_{\text{eff}} + l\omega_T + 2E_2)t_1 - 2E_2\tau_1] - \cos[(2\omega_{\text{eff}} + l\omega_T + 2E_2)t_2 - 2E_2\tau_1]}{2(2\omega_{\text{eff}} + l\omega_T + 2E_2)}$$

$$- R^s \frac{\cos[(2\omega_{\text{eff}} + l\omega_T - 2E_2)t_1 + 2E_2\tau_1] - \cos[(2\omega_{\text{eff}} + l\omega_T - 2E_2)t_2 + 2E_2\tau_1]}{2(2\omega_{\text{eff}} + l\omega_T - 2E_2)},$$

$$I_l^s(t_2, t_1, R^c, R^s, \omega_{\text{eff}}, E_2, \tau_1) \equiv \int_{t_1}^{t_2} \left[R^c \cos 2E_2(t - \tau_1) + R^s \sin 2E_2(t - \tau_1) \right] \sin(2\omega_{\text{eff}} + l\omega_T) t \, dt$$

$$= R^c \frac{\cos[(2\omega_{\text{eff}} + l\omega_T + 2E_2)t_1 - 2E_2\tau_1] - \cos[(2\omega_{\text{eff}} + l\omega_T + 2E_2)t_2 - 2E_2\tau_1]}{2(2\omega_{\text{eff}} + l\omega_T + 2E_2)}$$

$$+ R^c \frac{\cos[(2\omega_{\text{eff}} + l\omega_T - 2E_2)t_1 + 2E_2\tau_1] - \cos[(2\omega_{\text{eff}} + l\omega_T - 2E_2)t_2 + 2E_2\tau_1]}{2(2\omega_{\text{eff}} + l\omega_T - 2E_2)}$$

$$+ R^s \frac{\sin[(2\omega_{\text{eff}} + l\omega_T - 2E_2)t_2 + 2E_2\tau_1] - \sin[(2\omega_{\text{eff}} + l\omega_T - 2E_2)t_1 + 2E_2\tau_1]}{2(2\omega_{\text{eff}} + l\omega_T - 2E_2)}$$

$$- R^s \frac{\sin[(2\omega_{\text{eff}} + l\omega_T + 2E_2)t_2 - 2E_2\tau_1] - \sin[(2\omega_{\text{eff}} + l\omega_T + 2E_2)t_1 - 2E_2\tau_1]}{2(2\omega_{\text{eff}} + l\omega_T + 2E_2)}.$$

Then, the coefficients are

$$\bar{b} = \lim_{K \to \infty} \frac{1}{KT} \int_0^{KT} [C(t)^2 + D(t)^2] dt,$$

$$= \lim_{K \to \infty} \frac{1}{KT} \sum_{k=0}^{K-1} \int_{kT}^{kT+\tau_1} [C(t)^2 + D(t)^2] dt + \frac{1}{KT} \sum_{k=0}^{K-1} \int_{kT+\tau_1}^{(k+1)T} [C(t)^2 + D(t)^2] dt$$

$$= \lim_{K \to \infty} \frac{1}{KT} \sum_{k=0}^{K-1} \int_{kT}^{kT+\tau_1} (R_k^0 + R_k^c \cos 2E_1 t + R_k^s \sin 2E_1 t) dt$$

$$+ \lim_{K \to \infty} \frac{1}{KT} \sum_{k=0}^{K-1} \int_{kT+\tau_1}^{(k+1)T} [Q_k^0 + Q_k^c \cos 2E_2(t - \tau_1) + Q_k^s \sin 2E_2(t - \tau_1)] dt$$

$$= \lim_{K \to \infty} \frac{1}{KT} \sum_{k=0}^{K-1} \left[R_k^0 \tau_1 + Q_k^0 \tau_2 + I_0(kT + \tau_1, kT, R_k^c, R_k^s, E_1, 0) + I_0(kT + T, kT + \tau_1, Q_k^c, Q_k^s, E_2, \tau_1) \right],$$

$$c_l = \lim_{K \to \infty} \frac{2}{KT} \sum_{k=0}^{K-1} \left[I_l(kT + \tau_1, kT, 0, R_k^0, \omega_{\text{eff}}, 0) + I_l(kT + T, kT + \tau_1, 0, Q_k^0, \omega_{\text{eff}}, 0) \right.$$

$$+ I_l^s(kT + \tau_1, kT, R_k^c, R_k^s, \omega_{\text{eff}}, E_1, kT) + I_l^s(kT + T, kT + \tau_1, Q_k^c, Q_k^s, \omega_{\text{eff}}, E_2, \tau_1 + kT) \Big],$$

$$c_l' = \lim_{K \to \infty} \frac{2}{KT} \sum_{k=0}^{K-1} \Big[I_{l+1}(kT + \tau_1, kT, 0, R_k^0, 0, 0) + I_{l+1}(kT + T, kT + \tau_1, 0, Q_k^0, 0, 0)$$

$$+ I_{l+1}^s(kT + \tau_1, kT, R_k^c, R_k^s, 0, E_1, kT) + I_{l+1}^s(kT + T, kT + \tau_1, Q_k^c, Q_k^s, 0, E_2, \tau_1 + kT) \Big],$$

$$d_l = \lim_{K \to \infty} \frac{2}{KT} \sum_{k=0}^{K-1} \Big[I_l(kT + \tau_1, kT, R_k^0, 0, \omega_{\text{eff}}, 0) + I_l(kT + T, kT + \tau_1, Q_k^0, 0, \omega_{\text{eff}}, 0)$$

$$+ I_l^c(kT + \tau_1, kT, R_k^c, R_k^s, \omega_{\text{eff}}, E_1, kT) + I_l^c(kT + T, kT + \tau_1, Q_k^c, Q_k^s, \omega_{\text{eff}}, E_2, \tau_1 + kT) \Big],$$

$$d_l' = \lim_{K \to \infty} \frac{2}{KT} \sum_{k=0}^{K-1} \Big[I_{l+1}(kT + \tau_1, kT, R_k^0, 0, 0, 0) + I_{l+1}(kT + T, kT + \tau_1, Q_k^0, 0, 0, 0)$$

$$+ I_{l+1}^c(kT + \tau_1, kT, R_k^c, R_k^s, 0, E_1, kT) + I_{l+1}^c(kT + T, kT + \tau_1, Q_k^c, Q_k^s, 0, E_2, \tau_1 + kT) \Big]. \tag{31}$$

Note that all the integrals $I_l(\cdot)$, $I_l^c(\cdot)$, and $I_l^s(\cdot)$ are the superposition of trigonometric functions. By making use of summation formulas of trigonometric functions

$$\sum_{k=0}^{K} \cos kx = \frac{\sin \frac{x}{2} + \sin(\frac{1}{2} + K)x}{2 \sin \frac{x}{2}}, \quad \sum_{k=0}^{K} \sin kx = \frac{\cos \frac{x}{2} - \cos(\frac{1}{2} + K)x}{2 \sin \frac{x}{2}}, \tag{32}$$

one can obtain the limit results under concrete physical parameters. As an illustration, consider that $\theta_1 = \theta_2 = 0$, $\Delta_1 = 0$, $|\Delta_2| \gg |\epsilon_2|$, and $E_1 \tau_1 = E_2 \tau_2 = \pi/2$. Substituting those parameters into the expression (29), we have

$$P_{1 \to 2}(t) = \begin{cases} \frac{1}{2} - \frac{1}{2} \cos 2k\Theta \cos 2E_1 t, & t \in [kT, \tau_1 + kT), \\ \sin^2(k+1)\Theta \sin^2 E_2(t - \tau_1) + \cos^2 k\Theta \cos^2 E_2(t - \tau_1), & t \in [\tau_1 + kT, (k+1)T), \end{cases} \tag{33}$$

where $\Theta = \arccos \epsilon_2/E_2$. Then, according to Eq. (31), the coefficients in the Fourier transform become

$$\bar{b} = \lim_{K \to \infty} \frac{1}{KT} \int_0^{KT} P_{1 \to 2}^b(t) dt = \frac{1}{2},$$

$$c_0 = \lim_{K \to \infty} \frac{2}{KT} \int_0^{KT} P_{1 \to 2}^b(t) \sin(2\omega_{\text{eff}}) t dt \simeq \frac{1}{4} \frac{\Theta[1 + \cos \frac{2\tau_1}{T} \Theta]}{(\pi T/2\tau_1)^2 - \Theta^2},$$

$$d_0 = \lim_{K \to \infty} \frac{2}{KT} \int_0^{KT} P_{1 \to 2}^b(t) \cos(2\omega_{\text{eff}}) t dt \simeq -\frac{1}{4} \frac{\Theta \sin \frac{2\tau_1}{T} \Theta}{(\pi T/2\tau_1)^2 - \Theta^2},$$

$$c_{-1} = \lim_{K \to \infty} \frac{2}{KT} \int_0^{KT} P_{1 \to 2}^b(t) \sin(2\omega_{\text{eff}} - \omega_T) t dt \simeq \frac{1}{4} \frac{(\pi - \Theta)[1 + \cos \frac{2\tau_1}{T}(\pi - \Theta)]}{(\pi T/2\tau_1)^2 - (\pi - \Theta)^2},$$

$$d_{-1} = \lim_{K \to \infty} \frac{2}{KT} \int_0^{KT} P_{1 \to 2}^b(t) \cos(2\omega_{\text{eff}} - \omega_T) t dt \simeq -\frac{1}{4} \frac{(\pi - \Theta) \sin \frac{2\tau_1}{T}(\pi - \Theta)}{(\pi T/2\tau_1)^2 - (\pi - \Theta)^2}.$$

Hence, $b_0 = \sqrt{(c_0)^2 + (d_0)^2} \simeq 1/4$, $b_{-1} = \sqrt{(c_{-1})^2 + (d_{-1})^2} \simeq 1/4$. Therefore, the form of $P_{1 \to 2}(t)$ can be approximated as

$$P_{1 \to 2}(t) \simeq P_{1 \to 2}^m(t) = \frac{1}{2} - \frac{1}{4} \cos(2\omega_{\text{eff}} t) - \frac{1}{4} \cos(2\omega_{\text{eff}}^- t), \tag{34}$$

where $\omega_{\text{eff}}^- = \omega_T/2 - \omega_{\text{eff}}$. One can find that the transition probability shows the beat phenomenon in this parameter regime. Indeed, this is the Eq. (44) when we choose $N = 2$.

The numerical verification of the modified transition probability

In this section, we demonstrate that the dynamics of the periodic N-steps driven system can be well described by the modified transition probability formalism. First, we calculate the maximum transition probability $\mathcal{P}_s^{\text{max}}$ of the short time-scale dynamics. In principle, we can obtain the value of $\mathcal{P}_s^{\text{max}}$, according to the analytical expression of the micromotion operator $\mathcal{M}(t)$ given by Eq. (18). However, the expression is involved so that we cannot directly derive a the concise result. Here, we adopt an intuitive method to estimate $\mathcal{P}_s^{\text{max}}$. That is, we separately investigate

the dynamics of each Hamiltonian H_n $(n = 1, ..., N)$, and the maximum transition probability for each Hamiltonian H_n $(n = 1, ..., N)$ is

$$\mathcal{P}_{1\to2}^n(\tau_n) = \left(\frac{\epsilon_n}{E_n}\right)^2 \begin{cases} 1, & \tau_n \geq \frac{\pi}{2E_n}, \\ \sin^2(E_n\tau_n), & \tau_n < \frac{\pi}{2E_n}. \end{cases} \tag{35}$$

The maximum of $\mathcal{P}_{1\to2}^n(\tau_n)$ can be approximately regarded as the maximum transition probability of short time-scale dynamics:

$$\mathcal{P}_s^{\max} = \max\{\mathcal{P}_{1\to2}^n(\tau_n)\}. \tag{36}$$

On the other hand, the maximum transition probability for the long time-scale dynamics is $\mathcal{P}_l^{\max} = \epsilon_{\text{eff}}^2/E_{\text{eff}}^2$, where $E_{\text{eff}} = \sqrt{\epsilon_{\text{eff}}^2 + \Delta_{\text{eff}}^2/4}$. Therefore, we can rephrase that the actual dynamics of a TLS can be well described by the effective Hamiltonian in Eq. (19) for a full parameter range when $\mathcal{P}_s^{\max} \ll \mathcal{P}_l^{\max}$. If $\mathcal{P}_s^{\max} \simeq \mathcal{P}_l^{\max}$, the effective Hamiltonian derived by all methods (including the present method, the Floquet theory, and the Trotter expansion, etc.) is invalid, since the short time-scale dynamics would play a dominant role in the whole system dynamical evolution but the effective Hamiltonian does not contain any information of the short time-scale dynamics.

Generally speaking, it is meaningless to study the case where the transition probability $\mathcal{P}_l^{\max}$ is small, since it can be easily reached by the Hamiltonian H_n in the large-detuned regime. In the following, we consider the case where $\mathcal{P}_l^{\max} \simeq 1$, i.e., the long time-scale dynamics of the TLS is in the (near-) resonance regime. As a result, there is an additional restriction on the physical quantities. To address this issue in more detail, it is instructive to adopt the following definition,

$$\varepsilon^{\text{eff}}(t_s) = \frac{1}{t_s} \int_0^{t_s} \left| P_{1\to2}(t) - P_{1\to2}^{\text{eff}}(t) \right| dt, \tag{37}$$

where the transition probabilities $P_{1\to2}(t)$ and $P_{1\to2}^{\text{eff}}(t) = \frac{\epsilon_{\text{eff}}^2}{E_{\text{eff}}^2} \sin^2 E_{\text{eff}}t$ are given by the actual and predicted dynamics of the Hamiltonians $H(t)$ in Eq. (9) and the effective Hamiltonian in Eq. (19), respectively. Therefore, $\varepsilon^{\text{eff}}(t_s)$ represents the average error in the time interval $[0, t_s]$ when adopting the effective Hamiltonian to describe the actual dynamics. In a similar way, we employ $\varepsilon^{\text{m}}(t_s)$ to represent the average error in the time interval $[0, t_s]$ when adopting the modified transition probability to describe the actual dynamics, which reads

$$\varepsilon^{\text{m}}(t_s) = \frac{1}{t_s} \int_0^{t_s} |P_{1\to2}(t) - P_{1\to2}^m(t)| dt. \tag{38}$$

Taking the periodic two-steps driven system as an example, if the Hamiltonian H_1 is in the large-detuned regime $(|\Delta_1/\epsilon_1| \gg 1)$ and the Hamiltonian H_2 is in the (near-) resonance regime $(|\Delta_2/\epsilon_2| \simeq 0)$, the general form of $P_{1\to2}^m(t)$ is empirically written as

$$P_{1\to2}^m(t) = \frac{\epsilon_{\text{eff}}^2}{2(\epsilon_{\text{eff}}^2 + \Delta_{\text{eff}}^2/4)} \left[1 - (1-\lambda)\cos(2\omega_{\text{eff}}t) - \lambda\cos(2\omega_{\text{eff}}^-t) \right], \tag{39}$$

where $\omega_{\text{eff}}^- = \pi/T - \omega_{\text{eff}}$, and $\lambda = \mathcal{P}_s^{\max}(\pi - E_1\tau_1)/\pi$. In Figs. S1(a)-S1(b), we demonstrate $\varepsilon^{\text{eff}}(t_s)$ and $\varepsilon^{\text{m}}(t_s)$ as a function of Δ_1 and Δ_2, where $\tau_1 = 0.2$. We can observe in Fig. S1 that $\varepsilon^{\text{eff}}(t_s)$ is basically periodic with the variation of Δ_1. The reason can be found as follows. For each Hamiltonian H_n $(n = 1, ..., N)$, the evolution operator $U_n(t)$ satisfies: $U_n(t + k\pi/E_n) = \exp(ik\pi)U_n(t)$. Since the global phase can be ignored, the period of the dynamical evolution for each Hamiltonian H_n is π/E_n. In Fig. S2(a), we choose $k = 3$ and thus it has a cyclic evolution for the Hamiltonian H_2. Furthermore, comparing Fig. S1(a) and Fig. S1(b), we find that most regions can be well described by the modified transition probability in Eq. (39). To be specific, we divide the full parameter range into three regions:

(i) Region I: Both Hamiltonians H_1 and H_2 are in the large-detuned regime, $|\Delta_n/\epsilon_n| \gg 1$, $n = 1, 2$. It is observed in Figs. S1(a)-S1(b) that the maximum of $\varepsilon^{\text{eff}}(t_s)$ is not more than 0.075. Especially, we plot the actual dynamics and prediction dynamics in Fig. S2(a) when $\varepsilon^{\text{eff}}(t_s) = 0.029$, which shows that the actual dynamics of the TLS can be well described by the effective Hamiltonian in Eq. (19), as well as the modified transition probability in Eq. (39).

(ii) Region II: One of the Hamiltonians is in the large-detuned regime while the other is in the near-resonance regime, $|\Delta_1| \gg |\epsilon_1|$ and $|\Delta_2| \lessapprox |\epsilon_2|$ $(|\Delta_2| \gg |\epsilon_2|$ and $|\Delta_1| \lessapprox |\epsilon_1|)$. It is observed in Figs. S1(a)-S1(b) that the maximum of $\varepsilon^{\text{eff}}(t_s)$ is more than 0.2. Therefore, the effective Hamiltonian would be invalid to describe the actual dynamics of the system in some regions, as shown by the green-dashed curve in Fig. S2(b). However, the actual dynamics of the system can be well described by Eq. (39), as shown by the blue-dashed curve in Fig. S2(b).

(iii) Region III: Both Hamiltonians H_1 and H_2 are in the near-resonance regime, $|\Delta_n/\epsilon_n| \simeq 0$, $n = 1, 2$. It is observed in Figs. S1(a)-S1(b) that the modified formalism (39) is still suited for the description of the actual dynamics for most regions. Nevertheless, $\varepsilon^{\mathrm{m}}(t_s)$ is as high as 0.3 in few regions, which shows that the modified formalism (39) may not describe well the actual dynamics of the system. In those regions, the transition probability for short time-scales is large enough. Then, due to the effect of the short time-scale dynamics, $P_{1\to2}(t)$ reaches the maximum before the transition time $\mathbb{T} = 2\pi/\epsilon_{\mathrm{eff}}$, which would lead to the waveform distortion of dynamical evolution. As a result, we need to keep more terms in Eq. (30) to describe it, where the new term is $\omega_{\mathrm{eff}}^+ = \omega_T/2 + \omega_{\mathrm{eff}}$ (i.e., the term $l = 1$). As shown by the blue-dashed-line in Fig. S2(c), $P_{1\to2}^m(t)$ can well describe the actual dynamics now, since $\varepsilon^{\mathrm{m}}(t_s)$ is as low as 0.008.
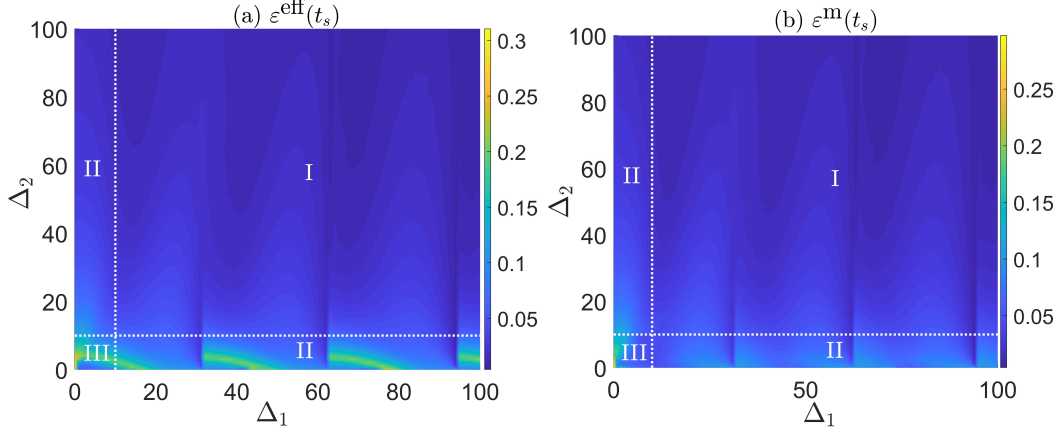

FIG. S1. The average error as a function of the detunings Δ_1 and Δ_2. (a) $\varepsilon^{\mathrm{eff}}(t_s)$ vs Δ_1 and Δ_2, (b) $\varepsilon^{\mathrm{m}}(t_s)$ vs Δ_1 and Δ_2, where $\tau_1 = 0.2$ and τ_2 is chosen to satisfy $\Delta_{\mathrm{eff}} = 0$. The other parameters are $N = 2$, $t_s = 100$, $t_p = 0$, $\epsilon_2 = 2$, $\theta_1 = 0$, $\theta_2 = \pi/3$ (in units of ϵ_1). It is shown that both the effective Hamiltonian in Eq. (19) and the modified transition probability in Eq. (39) can well describe the actual dynamics in Region I. The effective Hamiltonian is invalid but the modified transition probability is valid to describe the actual dynamics in Region II. The modified transition probability is also invalid to describe the actual dynamics in few area of Region III, because only two frequency terms is not enough and we need to keep more terms in Eq. (30).

The waveform for the beat phenomena

In this section, we briefly calculate the expression of the Hamiltonian which describes the quantum beat phenomenon in the TLS. Suppose that the general form of the time-dependent Hamiltonian reads

$$H(t) = \Delta(t)|2\rangle\langle2| + \epsilon(t)e^{i\theta(t)}|1\rangle\langle2| + \mathrm{H.c.}, \tag{40}$$

where the unknown coefficients $\Delta(t)$, $\epsilon(t)$, and $\theta(t)$ need to be solved.

First, when the transition probability exhibits beating, one type of the general forms can be written as

$$P_{1\to2}(t) = \frac{1}{2}(\sin^2 \epsilon_1 t + \sin^2 \epsilon_2 t). \tag{41}$$

where ϵ_1 and ϵ_2 are oscillation frequencies satisfying $|\epsilon_1 + \epsilon_2| \gg |\epsilon_1 - \epsilon_2|$. Since the expression of $P_{1\to2}(t)$ is given, we can preestablish the following ansatz for the wavefunction of the TLS

$$|\psi(t)\rangle = a_1(t)|1\rangle + a_2(t)|2\rangle, \tag{42}$$

where $a_1(t) = (\cos \epsilon_1 t + i\cos \epsilon_2 t)/\sqrt{2}$ and $a_2(t) = (\sin \epsilon_1 t + i\sin \epsilon_2 t)/\sqrt{2}$. Then, by substituting the wavefunction into the Schrödinger equation with the Hamiltonian given by Eq. (40), we obtain

$$\Delta(t) = \frac{(\epsilon_1 - \epsilon_2)\sin(\epsilon_1 + \epsilon_2)t}{\sin^2 \epsilon_1 t + \sin^2 \epsilon_2 t},$$

$$\epsilon(t) = \sqrt{\frac{\epsilon_1^2 \sin^2 \epsilon_1 t + \epsilon_2^2 \sin^2 \epsilon_2 t}{\sin^2 \epsilon_1 t + \sin^2 \epsilon_2 t}},$$
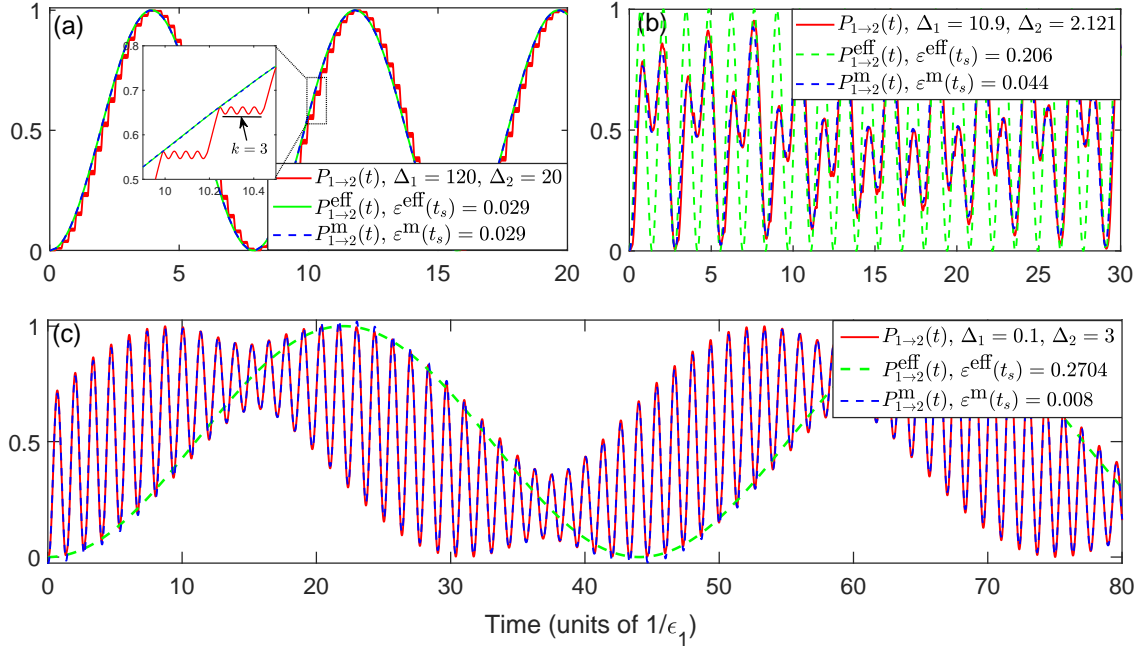
FIG. S2. $P_{1\to2}(t)$, $P_{1\to2}^{\text{eff}}(t)$, and $P_{1\to2}^{m}(t)$ as a function of evolution time t in different regions, where the parameters are $N = 2$, $t_s = 100$, $\epsilon_2 = 2$, $\theta_1 = 0$, $\theta_2 = \pi/3$ (in units of ϵ_1). (a) Region I, $\tau_1 = 0.2$. (b) Region II, $\tau_1 = 0.2$. (c) Region III, $\tau_1 = 0.1$. Notice that when we add the new term $l = 1$ in the modified transition probability, the prediction curve almost coincides with the actual dynamics in the noncompliance area of Region III.

$$\theta(t) = \arctan \frac{\epsilon_1 \sin^2 \epsilon_1 t + \epsilon_2 \sin^2 \epsilon_2 t}{(\epsilon_1 - \epsilon_2) \sin \epsilon_1 t \sin \epsilon_2 t}. \tag{43}$$

In Fig. S3 we plot the coefficients $\Delta(t)$, $\epsilon(t)$, and $\theta(t)$ as a function of the evolution time t. This figure shows that the waveforms are intricate. Particularly, $\Delta(t)$ and $\epsilon(t)$ would be singular at some moment. Therefore, the waveforms are hard to be achieved in experiments.

Beating in periodic N-steps driven system

In the main text, we demonstrate that the beat phenomena can appear in the periodic N-steps driven system. Without loss of generality, here we set $\theta_n = 0$ and study the situation where the beat phenomena is the most obvious. That is, there exists a complete transition in the periodic N-steps driven system ($\Delta_{\text{eff}} = 0$), and the transition probability can be approximately described by

$$P_{1\to2}^{m}(t) = \frac{1}{2}\left[\sin^2 \varpi_1(t - t_p) + \sin^2 \varpi_1'(t - t_p)\right], \tag{44}$$

where the frequencies ϖ_1 and ϖ_1' are closely related to the physical quantities of the periodic N-steps driven system, and t_p is the time-shifting factor.

First of all, we need to estimate the sum of all dynamical phases. If all Hamiltonians are in the large-detuned regime ($\left|\frac{\Delta_n}{\epsilon_n}\right| \gg 1$, $n = 1, 2, ..., N$), the following relations approximately hold on: $E_n = \sqrt{\epsilon_n^2 + \frac{\Delta_n^2}{4}} \simeq \frac{\Delta_n}{2}$ and $\frac{\epsilon_n}{E_n} \simeq 0$. Substituting into the equation $B_N(T) = 0$, we have $\sum_{n=1}^{N} E_n \tau_n \simeq k\pi$, $k = 1, 2, ...$ As a result, to implement a complete transition between levels, the accumulation of all dynamical phases approximately equal an integer multiple of π if all Hamiltonians are in the large-detuned regime. When N is an even number, the choice of physical quantities is quite obvious. That is, we can set each dynamical phase $E_n \tau_n = \frac{\pi}{2}$. Then we have $\sum_{n=1}^{N} E_n \tau_n = \frac{N\pi}{2}$, which satisfies the complete transition condition. At the same time, in order for beating to appear, one should guarantee that at least one Hamiltonian is in the resonance regime and the remainder Hamiltonian is in the large-detuned regime. Then, the
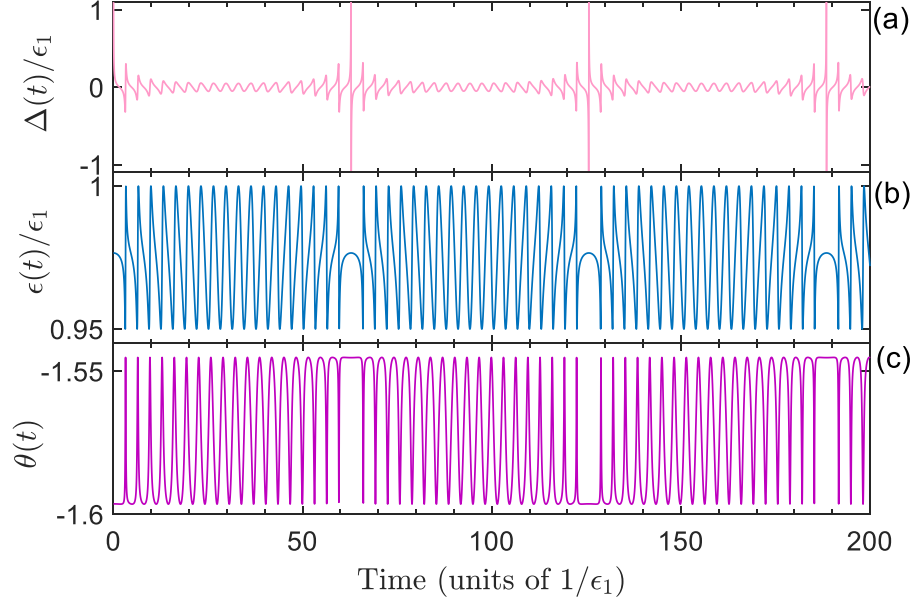
FIG. S3. The waveforms of different physical parameters to implement the beat phenomenon. (a) The detuning $\Delta(t)$ vs the time t. (b) The coupling strength $\epsilon(t)$ vs the time t. (c) The phase $\theta(t)$ vs the time t. $\epsilon_2 = 0.95\epsilon_1$. Note that the waveforms are intricate and singular at some moments in order to accurately achieve the beat phenomenon in the actual dynamics.

expressions of the frequencies ϖ_1 and ϖ_1' are empirically given by

$$\varpi_1 = \frac{1}{2} \begin{cases} (n_1 - 1)\epsilon'_{\text{eff}} + (n_1 + 1)\epsilon_{\text{eff}}, & n_1 \text{ is odd,} \\ n_1\epsilon'_{\text{eff}} + (n_1 - 2)\epsilon_{\text{eff}}, & n_1 \text{ is even,} \end{cases} \tag{45}$$

and

$$\varpi_1' = \frac{1}{2} \begin{cases} (n_1 + 1)\epsilon'_{\text{eff}} + (n_1 - 1)\epsilon_{\text{eff}}, & n_1 \text{ is odd,} \\ n_1\epsilon'_{\text{eff}} + (n_1 + 2)\epsilon_{\text{eff}}, & n_1 \text{ is even,} \end{cases} \tag{46}$$

where n_1 represents the number of Hamiltonians that are in the resonance regime.

Indeed, the beat phenomena always exists in the periodic N-steps driven system. Taking the two-steps sequence as an example, let us estimate the values of the frequencies ϖ_1 and ϖ_1'. Assume that the Hamiltonian H_1 is in the resonance regime and the Hamiltonian H_2 is in the large-detuned regime. We have $\Delta_1 = 0$ and $|\Delta_2/\epsilon_2| \gg 1$. Substituting those parameters into the expression (23), we find that the value of ϖ_1 can be approximated as

$$\varpi_1 = \epsilon_{\text{eff}} = \omega_{\text{eff}} = \frac{\arccos A_2(T)}{T} = \frac{\arccos\left[\frac{-\epsilon_2 \cos(\theta_1 - \theta_2)}{E_2}\right]}{T} = \frac{\arccos\left[\frac{-\epsilon_2 \cos(\theta_1 - \theta_2)}{\sqrt{\epsilon_2^2 + \Delta_2^2/4}}\right]}{T} \approx \frac{\pi}{2T}, \tag{47}$$

since $\epsilon_2/\sqrt{\epsilon_2^2 + \Delta_2^2/4} \approx 0$. Then, the value of ϖ_1' can be approximated as

$$\varpi_1' = \epsilon'_{\text{eff}} = \omega^-_{\text{eff}} = \frac{\omega_T}{2} - \epsilon_{\text{eff}} \approx \frac{\pi}{T} - \frac{\pi}{2T} = \frac{\pi}{2T}. \tag{48}$$

As a result, the frequencies $\varpi_1 = 2\epsilon_{\text{eff}}$ and $\varpi_1' = 2\epsilon'_{\text{eff}}$ are different but similar. Moreover, we have derived the expression of the transition probability in Eq. (34), which demonstrates that the amplitudes approximately equal each other. Thus the beating always exists in this system. In the similar derivative manner, one can obtain the same results when $N > 2$.

We plot in Fig. S4(a) the average error $\varepsilon^{\text{m}}(t_s)$ as a function of Δ_6 for different n_1. These results demonstrate that Eq. (44) with the frequencies ϖ_1 and ϖ_1' given by Eqs. (45)-(46) can be used to describe well the actual dynamics of the periodic N-steps driven system, because the maximum value of $\varepsilon^{\text{m}}(t_s)$ is no larger than 0.066. As examples, we plot in Figs. S4(b)-S4(c) the actual and predicted dynamical evolution of system when $n_1 = 1$ and $n_1 = 2$, respectively.

When N is an odd number, the choice of physical quantities is slightly different from the even N case. That is, the dynamical phase caused by one Hamiltonian H_{k_0} should satisfy $E_{k_0}\tau_{k_0} = \pi$, while the remaining still satisfy $E_n\tau_n = \frac{\pi}{2}$ ($n \neq k_0$). Thus we can consider two cases according to the Hamiltonian H_{k_0}.
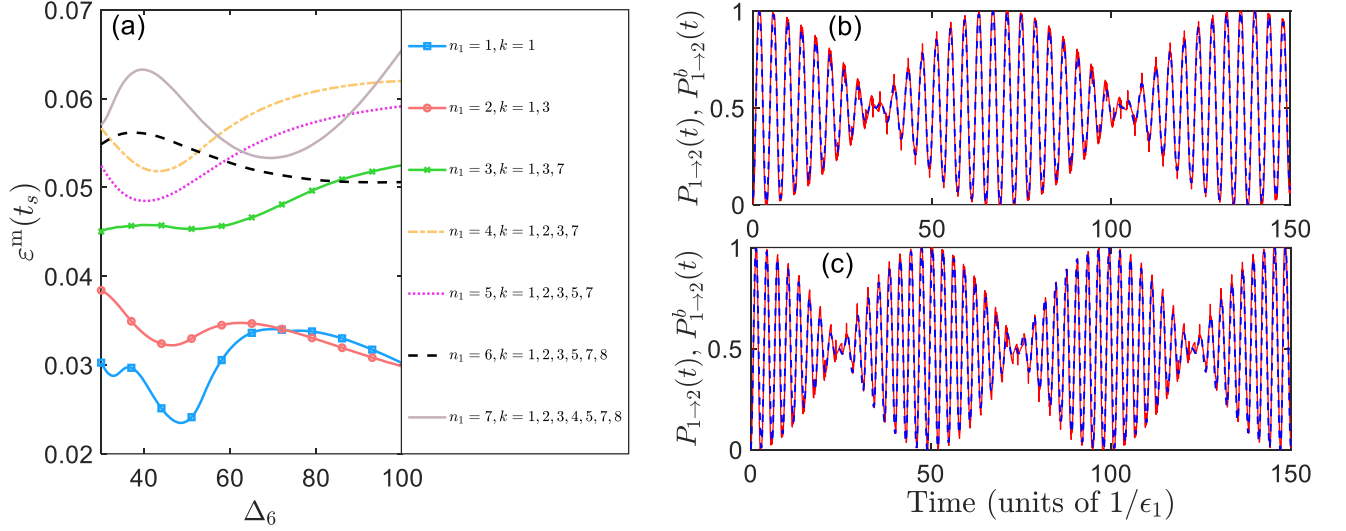
FIG. S4. (a) $\varepsilon^{\mathrm{m}}(t_s)$ vs Δ_6 with different n_1 in a periodic N-steps driven system, where $N = 8$ and we randomly select a set of physical quantities (in units of ϵ_1): $\epsilon_2 = 1.8$, $\epsilon_3 = 1.5$, $\epsilon_4 = 1.1$, $\epsilon_5 = 1.2$, $\epsilon_6 = 1.6$, $\epsilon_7 = 1.9$, $\epsilon_8 = 1.3$, $\Delta_1 = 0$, $\Delta_2 = 67$, $\Delta_3 = 60$, $\Delta_4 = 46$, $\Delta_5 = 83$, $\Delta_6 = 36$, $\Delta_7 = 40$, $\Delta_8 = 91$. In the legend, each k indicates that the k-th Hamiltonian is in the resonance regime. (b)-(c) The time-dependent transition probability $P_{1\to 2}(t)$ with (b) $n_1 = 1$, (c) $n_1 = 2$ in a periodic N-steps driven system, where the red-line represents the actual dynamics and the blue-dashed-line corresponds to the predictions given by Eq. (44). Those results show that when N is even, the actual dynamics can be well described by the beating formula (44) with the frequencies (45)-(46).

(i) The Hamiltonian H_{k_0} is in the large-detuned regime. One easily finds that the evolution operator of the Hamiltonian H_{k_0} is an identity operator, thus it does not affect the system dynamics. On the other hand, due to the large-detuned regime, the transition probability caused by this Hamiltonian is small enough. Thus, we can ignore this Hamiltonian and regard the N-steps driven system as an $(N-1)$-steps driven system. As a result, the expressions of coefficients ϖ_1 and ϖ_1' in this case is the same to the situation where N is an odd number, which is governed by Eqs. (45)-(46).

(ii) The Hamiltonian H_{k_0} is in the resonance regime. In this case, the dynamical phase caused by the Hamiltonian H_{k_0} is twice over the dynamical phase caused by the Hamiltonian in the situation where N is an odd number. Therefore, when the number of Hamiltonians that are in the resonance regime is n_1, we should substitute $(n_1 + 1)$ into Eqs. (45)-(46) to achieve the expressions of the frequencies ϖ_1 and ϖ_1'. As a result, in this case the expressions can be written as

$$\varpi_1 = \frac{1}{2} \begin{cases} (n_1 + 1)\epsilon_{\mathrm{eff}}' + (n_1 - 1)\epsilon_{\mathrm{eff}}, & n_1 \text{ is odd}, \\ n_1\epsilon_{\mathrm{eff}}' + (n_1 + 2)\epsilon_{\mathrm{eff}}, & n_1 \text{ is even}, \end{cases} \tag{49}$$

and

$$\varpi_1' = \frac{1}{2} \begin{cases} (n_1 + 1)\epsilon_{\mathrm{eff}}' + (n_1 + 3)\epsilon_{\mathrm{eff}}, & n_1 \text{ is odd}, \\ (n_1 + 2)\epsilon_{\mathrm{eff}}' + n_1\epsilon_{\mathrm{eff}}, & n_1 \text{ is even}. \end{cases} \tag{50}$$

We also plot in Fig. S5(a) the average error $\varepsilon^{\mathrm{m}}(t_s)$ as a function of Δ_7 with different n_1. It demonstrates that the Eq. (44) with the frequencies ϖ_1 and ϖ_1' given by Eqs. (49)-(50) can be used to describe well the actual dynamics of the periodic N-steps driven system, since the maximum value of $\varepsilon^{\mathrm{m}}(t_s)$ is no larger than 0.082. As examples, we plot in Figs. S5(b)-S5(c) the actual and predicted dynamical evolution of system when $n_1 = 2$ and $n_1 = 3$, respectively.
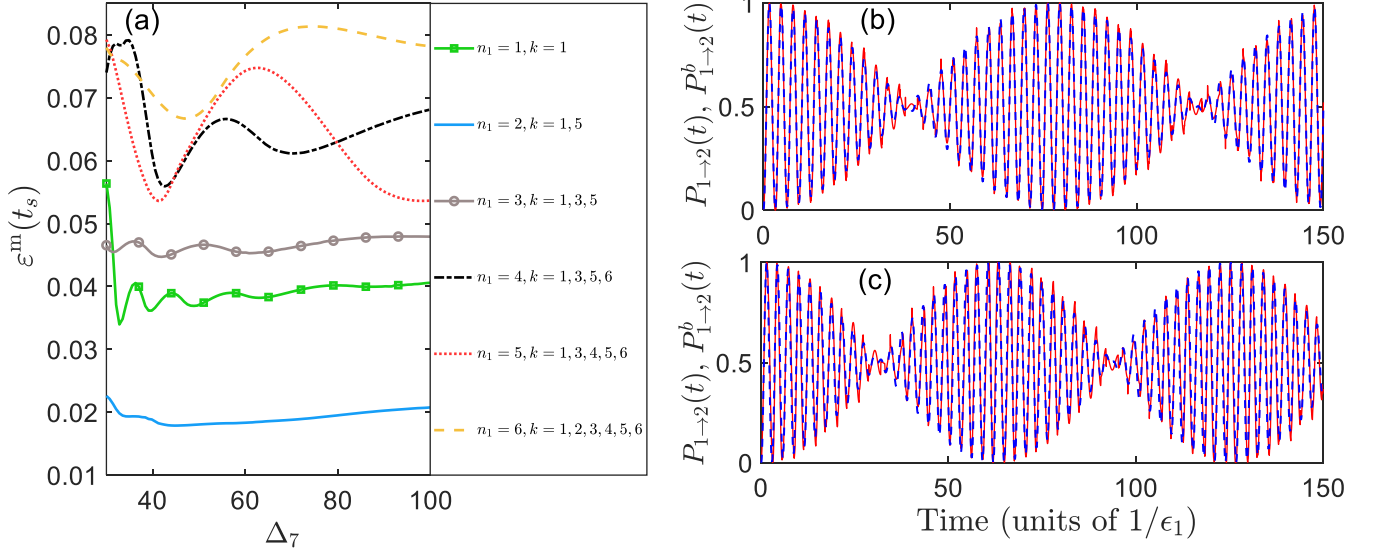
FIG. S5. (a) $\varepsilon^{\mathrm{m}}(t_s)$ vs Δ_6 with different n_1 in a periodic N-steps driven system, where $N = 7$ and we randomly select a set of physical quantities (in units of ϵ_1): $\epsilon_2 = 1.8$, $\epsilon_3 = 1.5$, $\epsilon_4 = 1.1$, $\epsilon_5 = 1.2$, $\epsilon_6 = 1.6$, $\epsilon_7 = 1.9$, $\epsilon_8 = 1.3$, $E_1 \tau_1 = \pi$, $\Delta_1 = 0$, $\Delta_2 = 55$, $\Delta_3 = 62$, $\Delta_4 = 47$, $\Delta_5 = 88$, $\Delta_6 = 35$, $\Delta_7 = 65$. In the legend, each k indicates that the k-th Hamiltonian is in the resonance regime. The time-dependent transition probability $P_{1 \to 2}(t)$ with (b) $n_1 = 2$, (c) $n_1 = 3$ in the periodic N-steps driven system, where the red-line represents the actual dynamics and the blue-dashed-line corresponds to the predictions given by Eq. (44). Those results show that when N is odd, the actual dynamics can be well described by the beating formula (44) with the frequencies (49)-(50).